Development of Lower-Energy Photosensitizer for Photocatalytic CO_2 Reduction: Modification of Porphyrin Dye in Hybrid Catalyst System

Dong-Il Won, Jong-Su Lee, Qiankai Ba, Yang-Jin Cho, Ha-Yeon Cheong, Sunghan Choi, Chul Hoon Kim,* Ho-Jin Son,* Chyongjin Pac, and Sang Ook Kang*

Department of Advanced Materials Chemistry, Korea University, Sejong 30019, Korea.

*Correspondence and requests for materials should be addressed to
*E-mail: Ho-Jin Son: hjson@korea.ac.kr
*E-mail: Chul Hoon Kim: chulhoon@korea.ac.kr
*E-mail: Sang Ook Kang: sangok@korea.ac.kr

Table of contents

General Procedures

All reagents were purchased from Aldrich and used without further purification. Chemicals for analytical measurements were of the highest available purity. Hombikat UV-100 TiO_2 particles (100% anatase) were purchased from Huntsman P&A GmbH. All manipulations were performed under a dry nitrogen or argon atmosphere by using standard Schlenk techniques. Tetrahydrofuran (THF) and toluene (Tol) were distilled from sodium benzophenone. *N,N*-Dimethylformamide (DMF) was distilled from calcium hydride and stored over molecular sieves. Dichloromethane (MC) and acetonitrile (CH_3CN) were refluxed over and distilled from phosphorus pentoxide (P_2O_5) before use. The ^1H and ^{13}C NMR spectra were recorded on a Varian Mercury 300 spectrometer (operating at 300.1 and 75.4 MHz) and Bruker Ascend 400 spectrometer in KBSI Ochang Center (operating at 400.1 MHz and 100.6 MHz), respectively. Proton and carbon chemical shifts were referenced relative to the corresponding solvent signals, δ H 7.26 and δ C 77.16 of chloroform-*d* and δ H 8.62, 7.29, and 7.68 and δ C 150.35, 135.91, and 123.87 of pyridine-d_5. The absorption and photoluminescence spectra were recorded on a Shimadzu UV-3101PC UV/Vis/NIR scanning spectrophotometer, a Agilent Technologies Cary 5000 UV-Vis-NIR spectrophotometer and a VARIAN Cary Eclipse fluorescence spectrophotometer, respectively. The diffuse reflectance UV-visible absorption spectra of powder samples were recorded on a Scinco spectrophotometer S-3100. The IR spectra were taken on a Cary 660 FTIR spectrometer. Cyclic voltammetry (CV) measurements were carried out for THF and MC solutions of the **ZnPs** (1 mM) in the presence of tetrabutylammonium perchlorate (0.1 M) at room temperature using a BAS 100B electrochemical analyzer equipped with a glassy carbon working electrode, a platinum wire counter electrode, and an Ag|AgCl or a SCE reference. All gaseous and liquid products produced from photoreaction were analyzed by gas chromatography (GC) and Waters high-performance liquid chromatography (HPLC) equipped with Rspak KC-811 column, respectively.

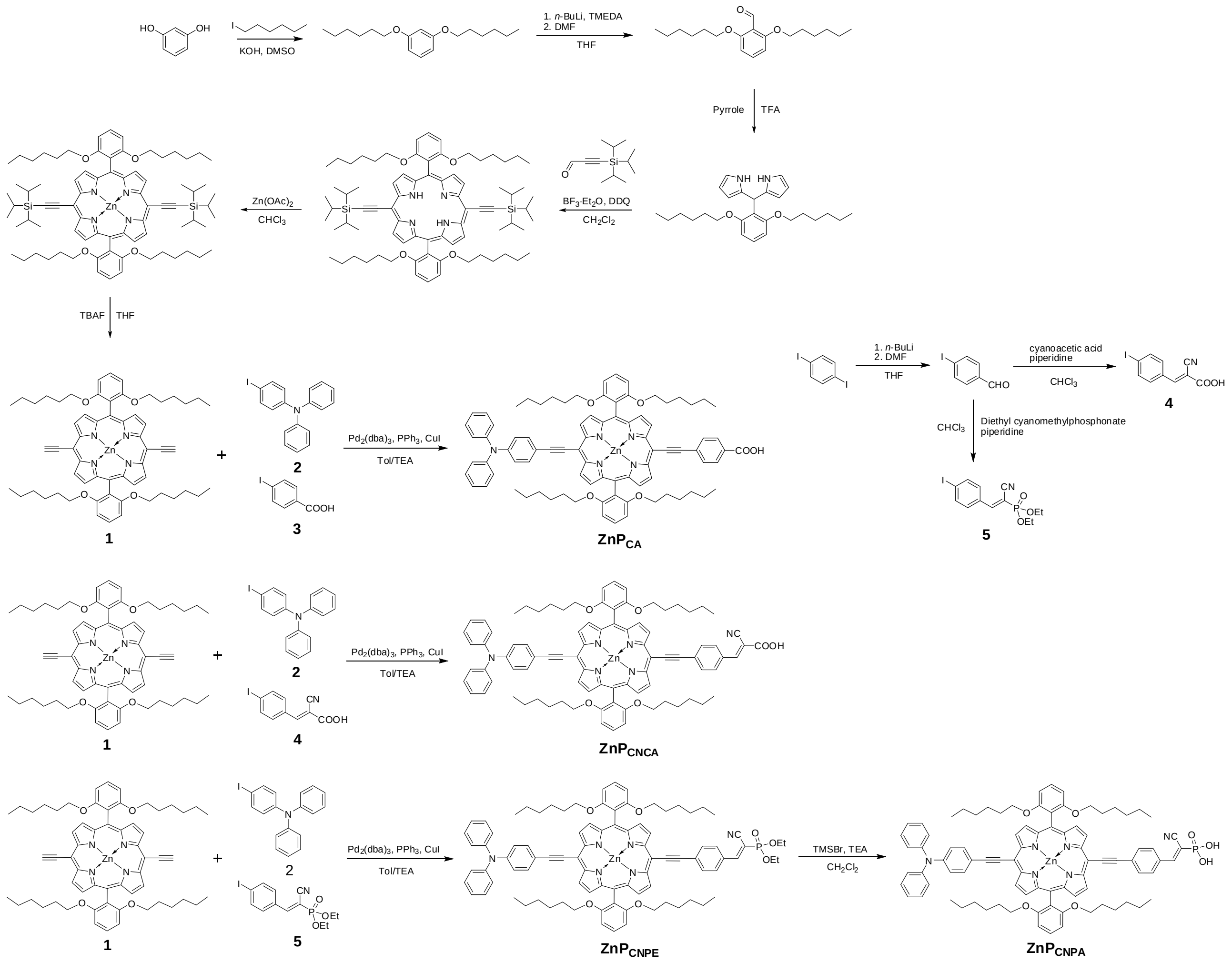

Scheme S1. Synthetic routes of the Zn-porphyrin antenna (**ZnPs**).

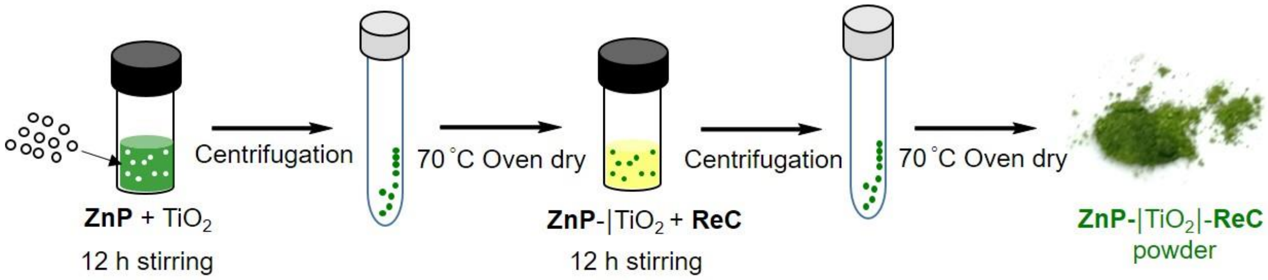

Figure S1. Schematic description of sequential adsorption process for immobilization of **ZnPs** and **ReC** on TiO_2 particles.

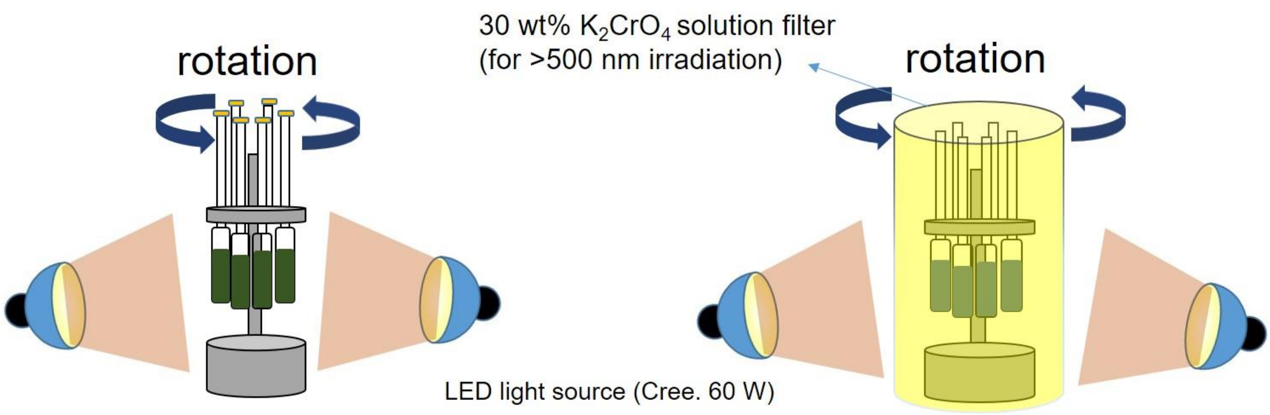

Figure S2. Schematic description of the homemade merry-go-round irradiation apparatus.

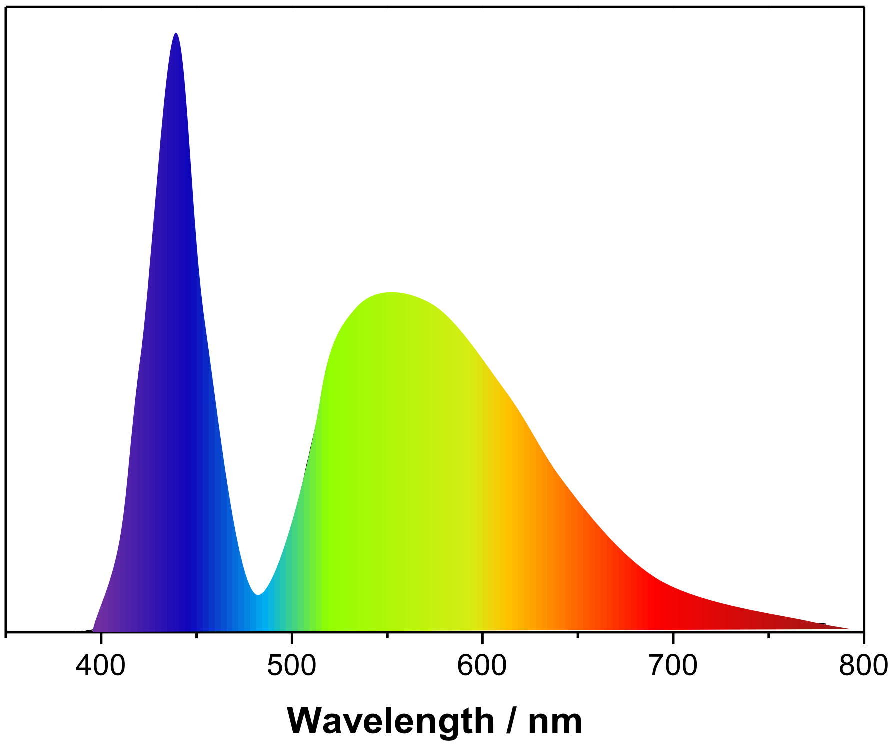

Figure S3. Spectrum of the LED lamp (Cree. 60 W) used as a light source in this study.

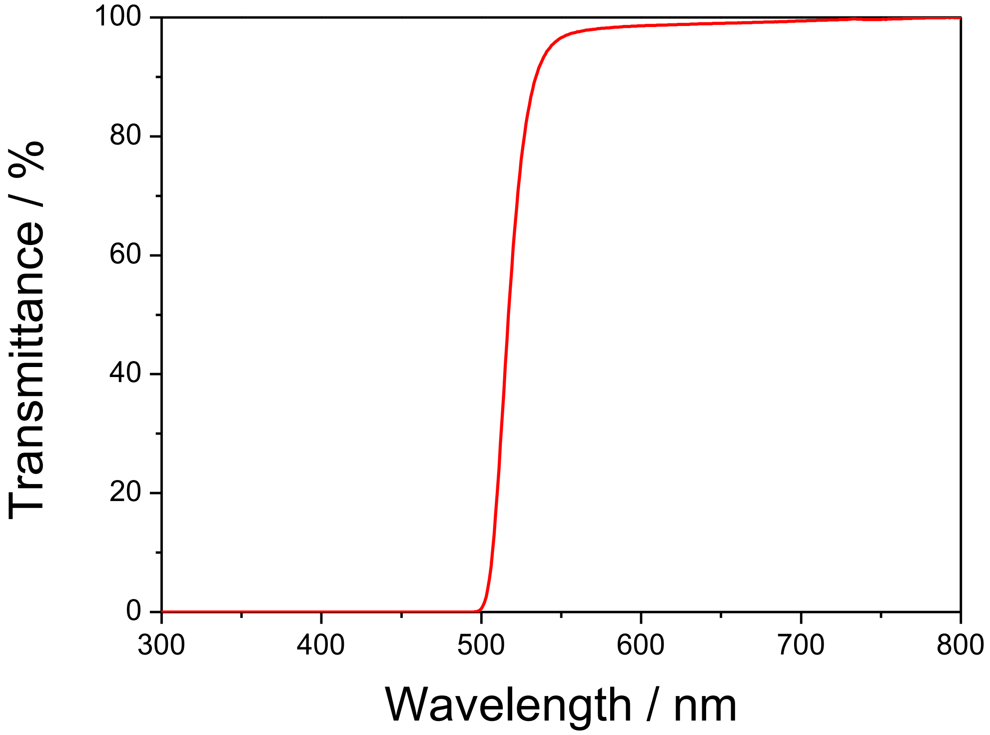

Figure S4. Transmittance of 30 wt% K_2CrO_4 solution filter irradiation (1 cm path length of light).

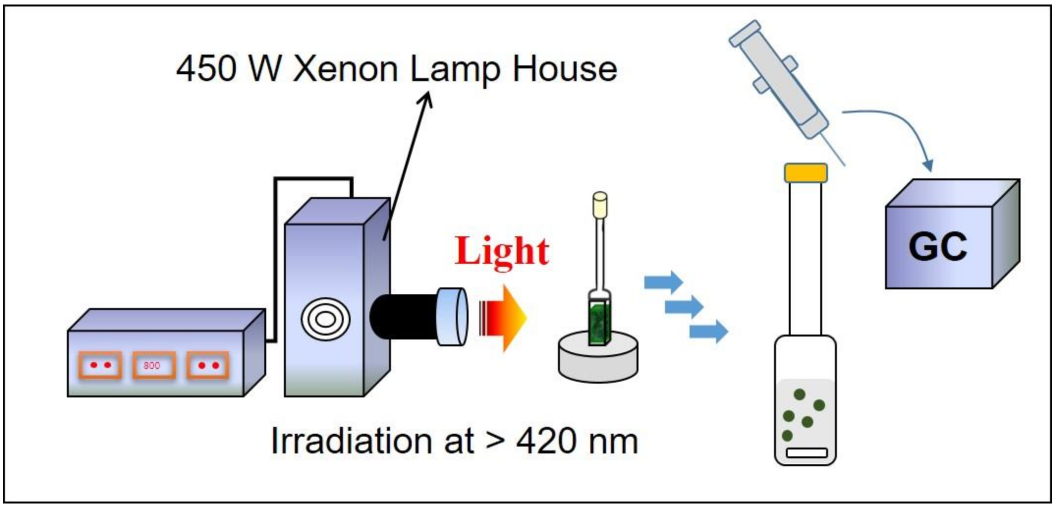

Figure S5. Schematic description of the 450 W Xenon lamp irradiation apparatus.

The Effect of Different Dye and Catalyst Loading Amounts in Photocatalysis: The dye and catalyst loading amount have been optimized by checking the photocatalytic CO_2 reduction activities in our homemade merry-go-round apparatus; LED irradiation (Cree, 60 W, λ >500 nm) of 10 mg **ZnP$_{\mathbf{CNCA}}$**(0.38 to 1.5 μmol)-|TiO_2(10 mg)|-**ReC**(0.1 to 0.3 μmol) and 0.1 M BIH (SED) in 3 mL DMF/H_2O mixture solvent (2.5 vol% water). As shown in Figure S6 (see below), the increase of TON_{Re} with the variation of **ZnP$_{\mathbf{CNCA}}$** loading amount from 0.38 to 1.5 μmol was stopped with increase of **ZnP$_{\mathbf{CNCA}}$** loading amount (0.75 μmol). Meanwhile, it is observed that the activity of photo-generated CO per **ReC** (TON_{Re}) is almost constant with increasing amount of **ReC** (0.1 to 0.3 μmol/10 mg dye/TiO_2). This result is in contrast to the expectation that the increase of **ReC** loading amount will counterbalance the lopsided electron flow dynamics in this ternary system because the electron transfer rate from TiO_2 to **ReC** (~ms) is known to be much slower than from the anchored dye to TiO_2 (~fs).[1,2] Such less sensitivity of **ReC** loading amount is believed to be due to a very slow chemical process at the Re(I) catalytic site.[1,3] The CO formation (CO / μmol per 10 mg hybrid catalyst) increases with the increase of absolute amount of Re(I) catalytic sites (**ReC**) (see the inset of Figure S7).

[1] Abdellah, M.; El-Zohry, A. M.; Antila, L. J.; Windle, C. D.; Reisner, E.; Hammarström, L. *J. Am. Chem. Soc.* **2017**, *139*, 1226−1232.

[2] Reynal, A.; Lakadamyali, F.; Gross, M. A.; Reisner, E.; Durrant, J. R. *Energy. Environ. Sci.* **2013**, *6*, 3291−3300.

[3] Windle, C. D.; Pastor, E.; Reynal, A.; Whitwood, A. C.; Vaynzof, Y.; Durrant, J. R.; Perutz, R. N.; Reisner, E. *Chem. - Eur. J.* **2015**, *21*, 3746−3754.

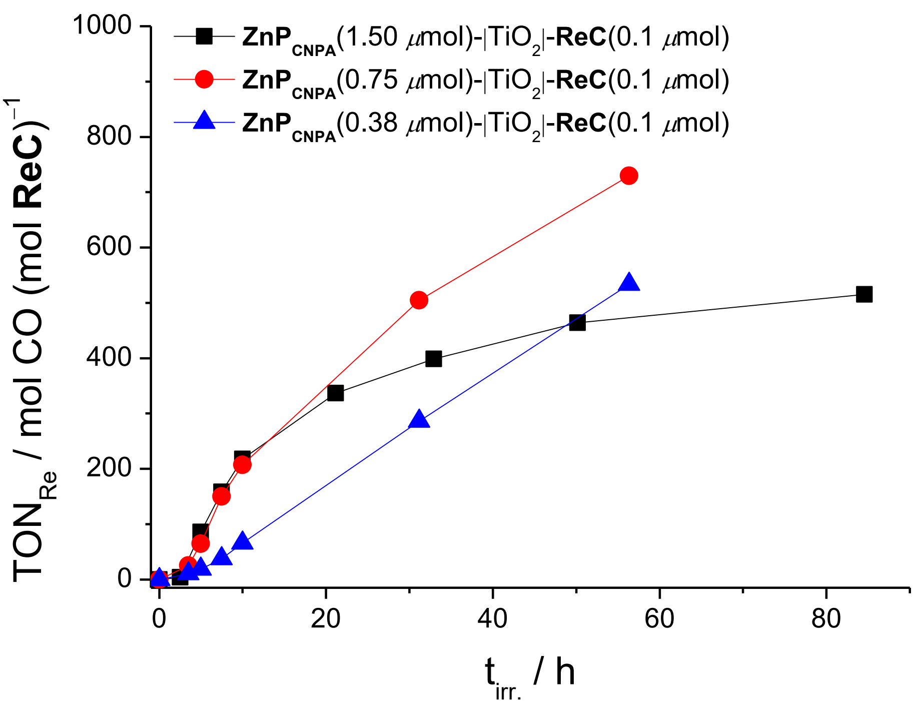

Figure S6. Time courses of CO production by irradiation at >400 nm for **ZnP$_{CNCA}$**-|TiO$_2$|-**ReC** with the variation of **ZnP$_{CNCA}$** loading amount from 0.38 to 1.50 μmol; LED irradiation (Cree, 60 W, λ > 500 nm) of 10 mg **ZnP$_{CNCA}$**(0.38 to 1.5 μmol)-|TiO$_2$(10 mg)|-**ReC**(0.1 μmol) and 0.1 M BIH (SED) in 3 mL DMF/H_2O mixture solvent (2.5 vol% water).

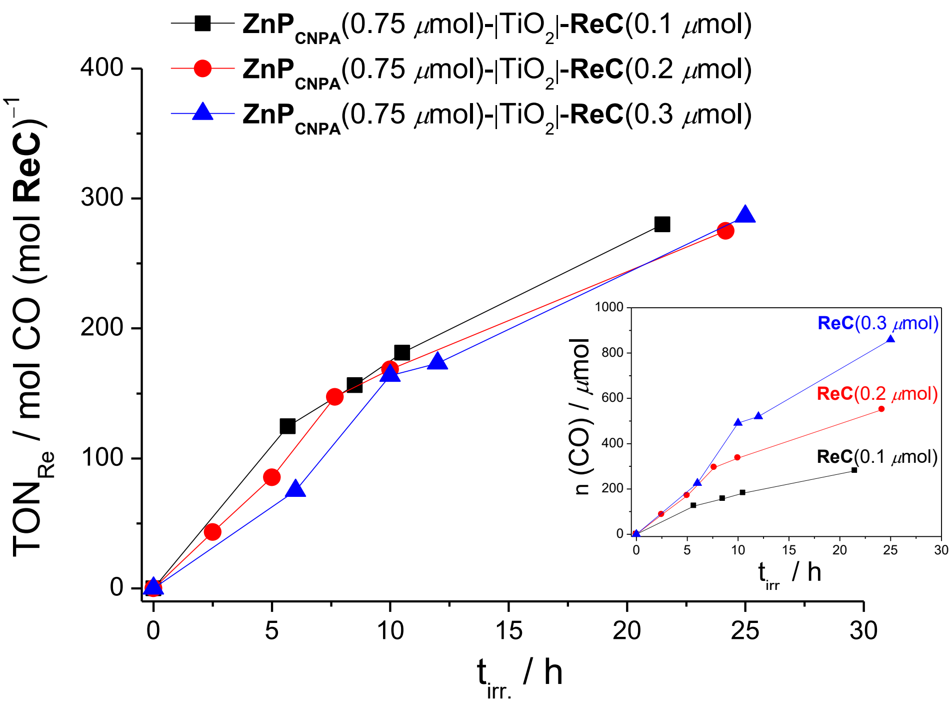

Figure S7. Visible light driven CO production per Re(I) catalyst (TON_{Re}) with porphyrin-sensitized TiO_2 nanoparticles (**ZnP$_{CNPA}$**(0.75 *μ*mol)-|TiO_2|-**ReC**(*x* *μ*mol)) prepared with the variation of **ReC** loading amount (0.1 *μ*mol to 0.3 *μ*mol) in DMF/H_2O mixture solvent (2.5 vol% water) (3 mL) in the presence of 0.1 M BIH. Inset shows the total amount of CO evolution (*μ*mol) per TiO_2 particle.

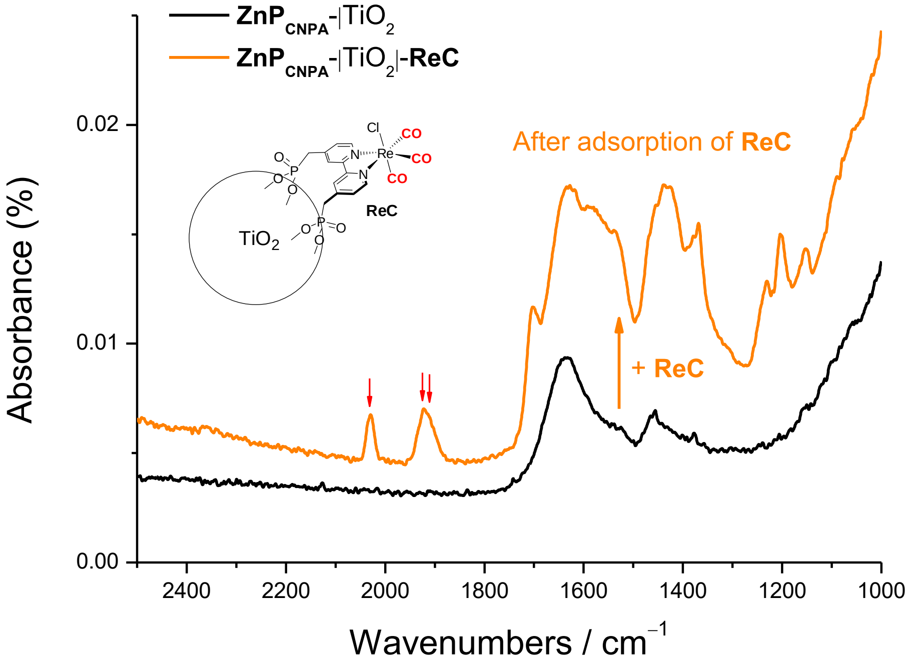

Figure S8. IR spectra of **ZnP$_{CNPA}$-**|TiO$_2$ and **ZnP$_{CNPA}$-**|TiO$_2$|**-ReC** in KBr discs (sample: KBr ≈ 1:100). The IR spectrum shows the distinct absorption bands at 2028 and 1894–1920 cm^{-1}, which is derived from the presence of CO ligands of **ReC**.

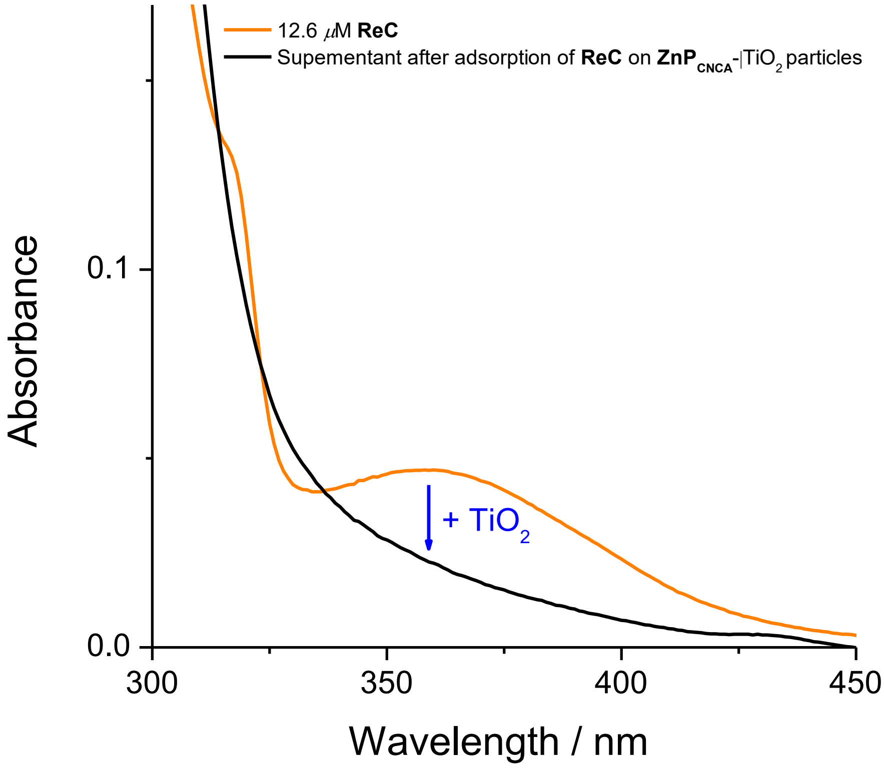

Figure S9. Comparison of absorption spectra of catalyst solution before (orange line) and after (black line) adsorption process of **ReC** with **ZnP**$_{\mathbf{CNCA}}$-|TiO_2 particles. Almost complete absence of **ReC** absorption bands is observed after the adsorption process, indicating the successful loading of added **ReC** (0.1 μmol) on **ZnP**$_{\mathbf{CNCA}}$-|TiO_2 particles.

The determination of ZnP and Re(I) catalyst coverage on TiO_2: The degree of coverage of porphyrin dyes and catalysts (**ZnP** and **ReC**) on TiO_2 surface is calculated using the following method: the area of Dye or catalysts adsorbed on 10 mg of TiO_2)/2.5 m^2 (surface area of 10 mg of TiO_2) = coverage.

	Area of components loaded on 10 mg TiO_2 (m^2)	Coverage (area of components/2.5 m^2)
ZnP	6.3×10^{-1}	0.25
ReC	2.0×10^{-2}	0.01

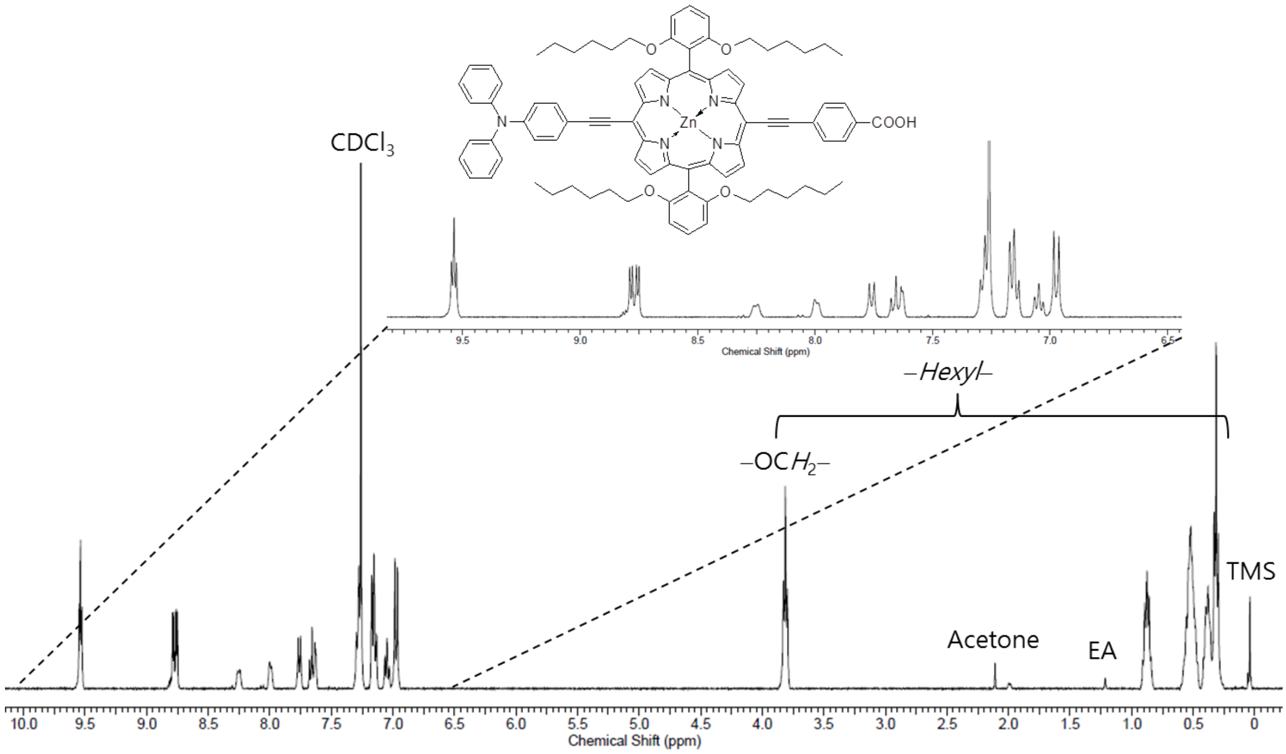

Figure S10. [1]H-NMR of **ZnP$_{CA}$**.

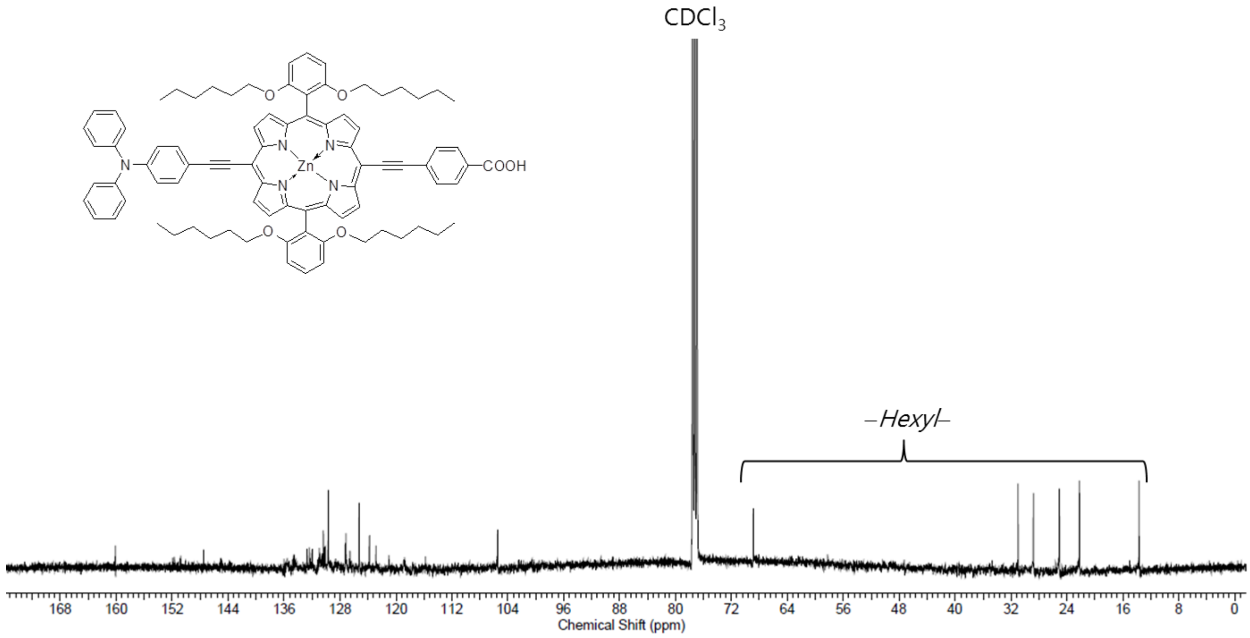

Figure S11. ^{13}C-NMR of **ZnP$_{CA}$**.

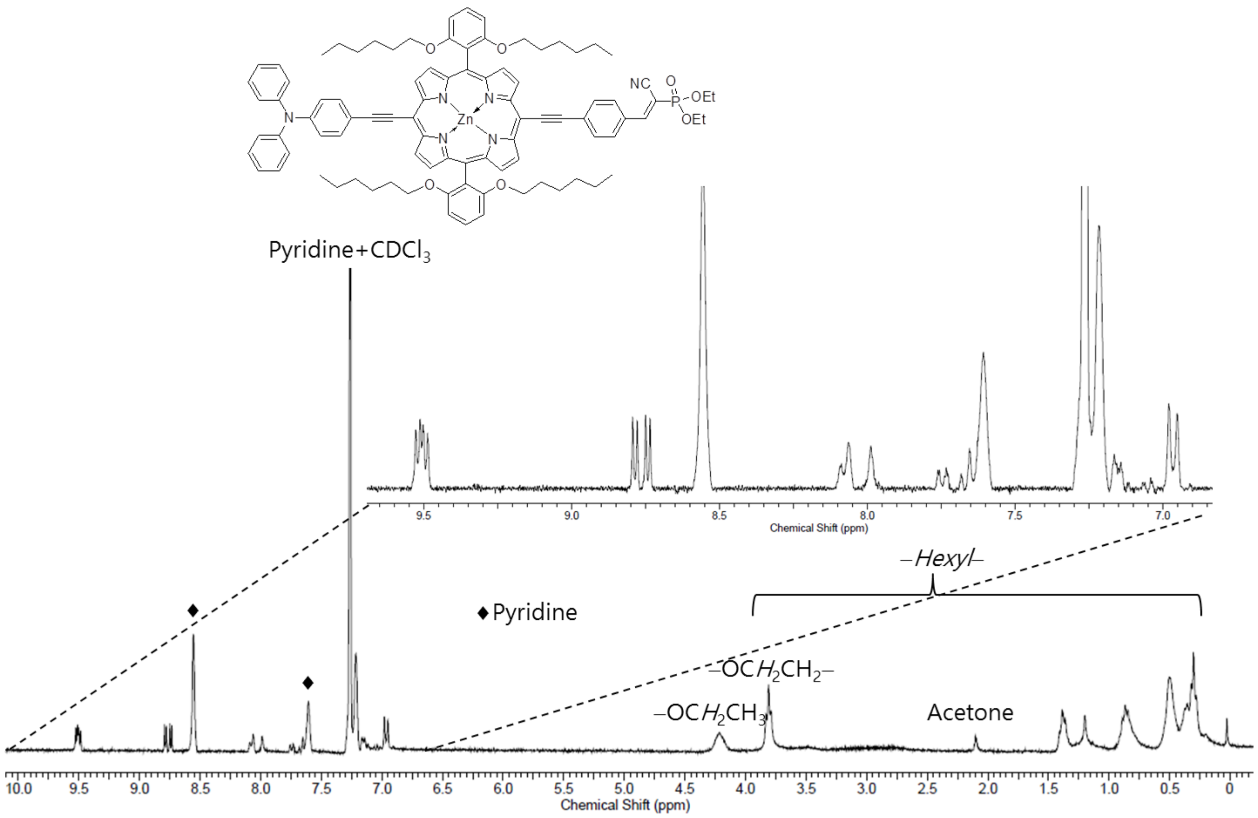

Figure S12. ^{1}H-NMR of **ZnP$_{\mathbf{CNPE}}$**.

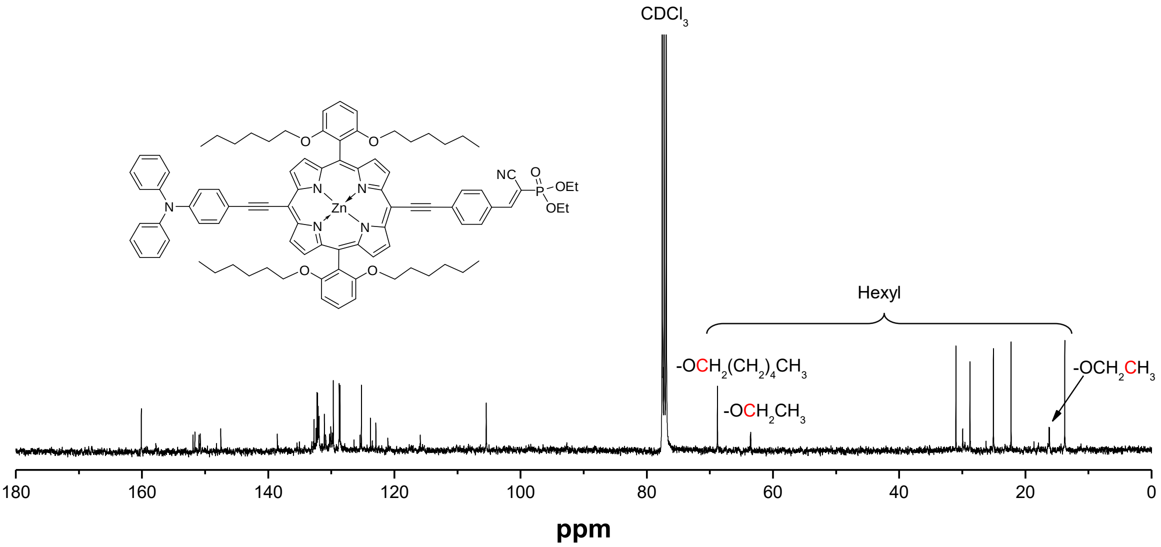

Figure S13. ^{13}C-NMR of **ZnP$_{\mathbf{CNPE}}$**.

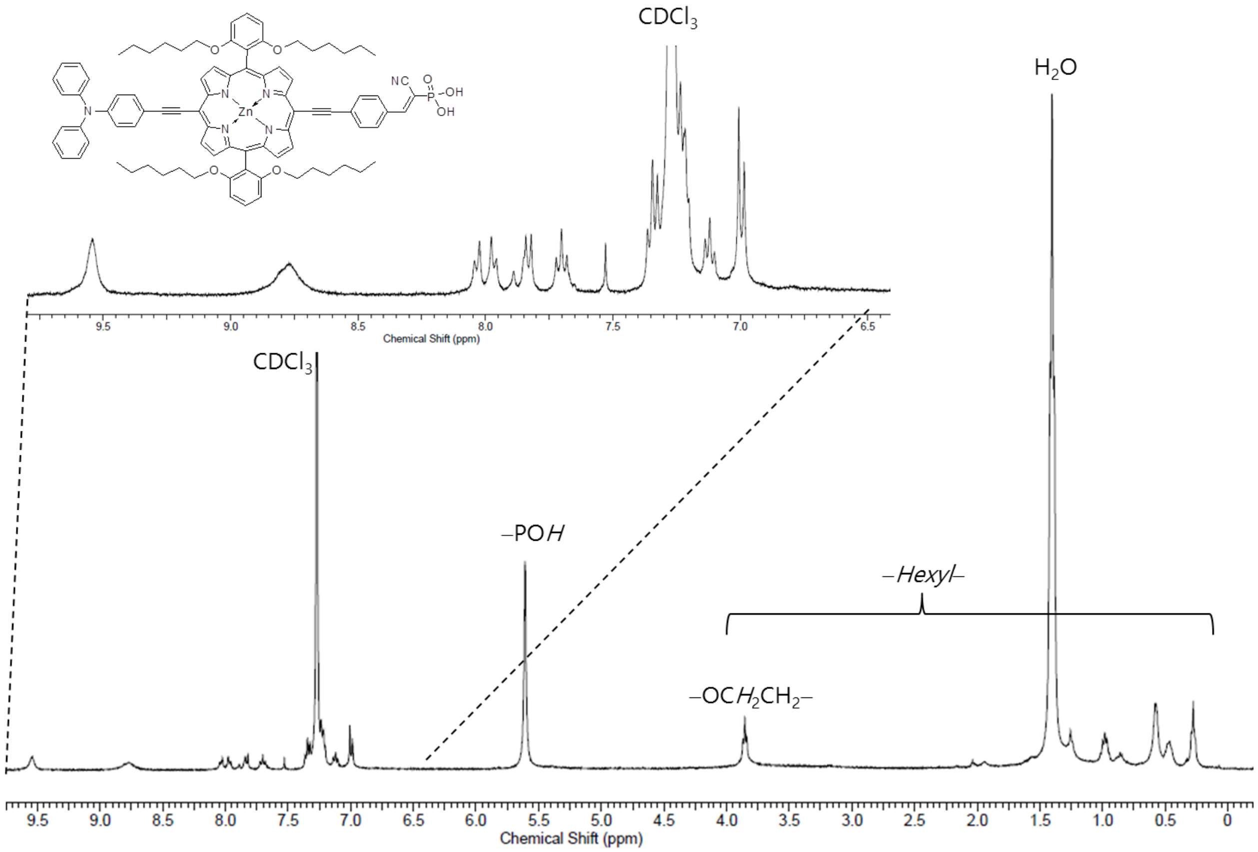

Figure S14. ^{1}H-NMR of **ZnP$_{\mathbf{CNPA}}$**.

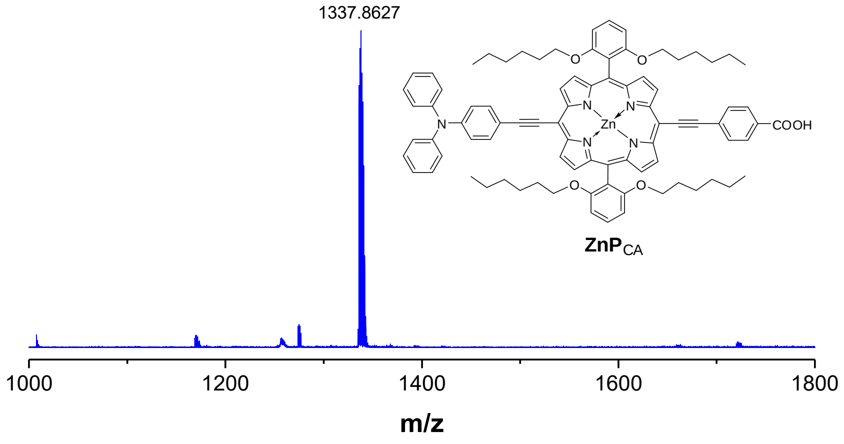

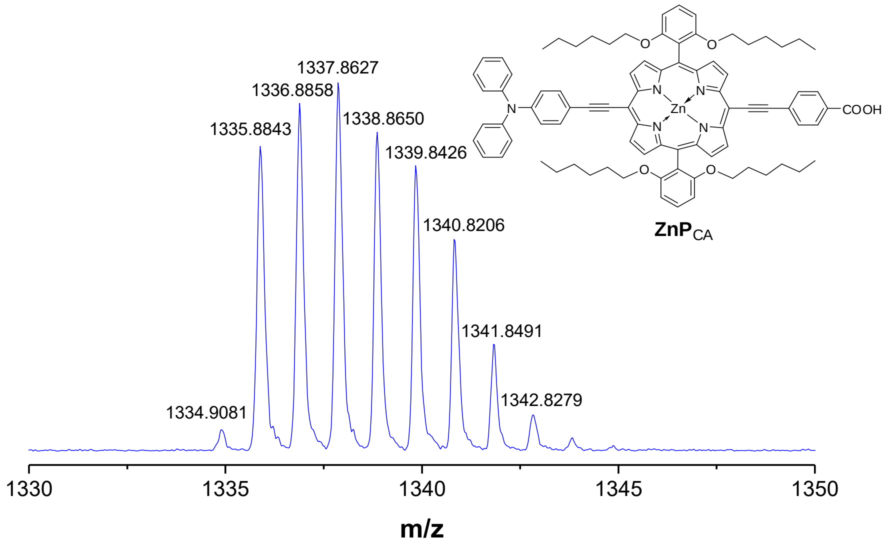

Figure S15. MALDI-TOF mass spectra of $\mathbf{ZnP_{CA}}$.

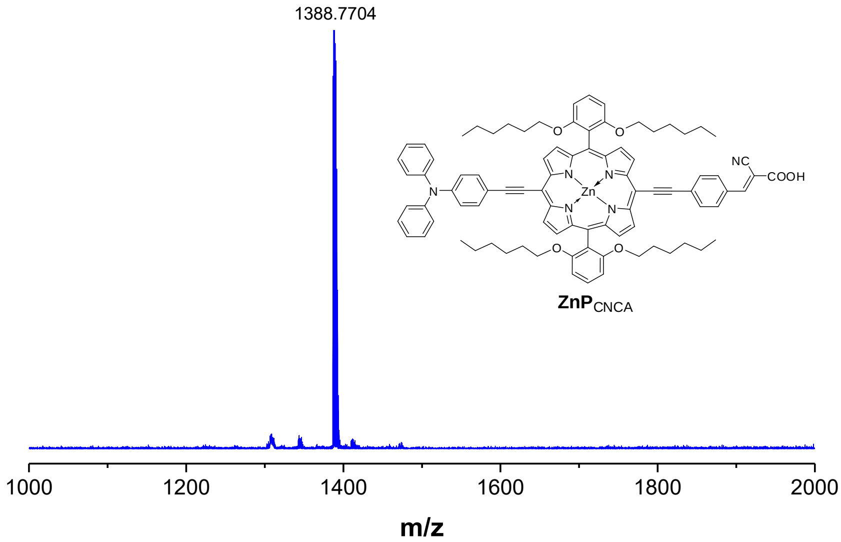

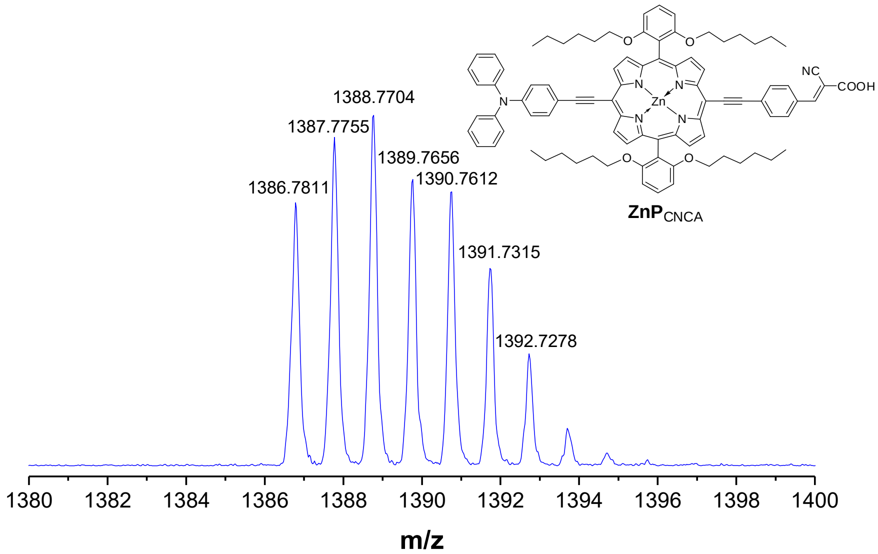

Figure S16. MALDI-TOF mass spectra of **ZnP$_{CNCA}$**.

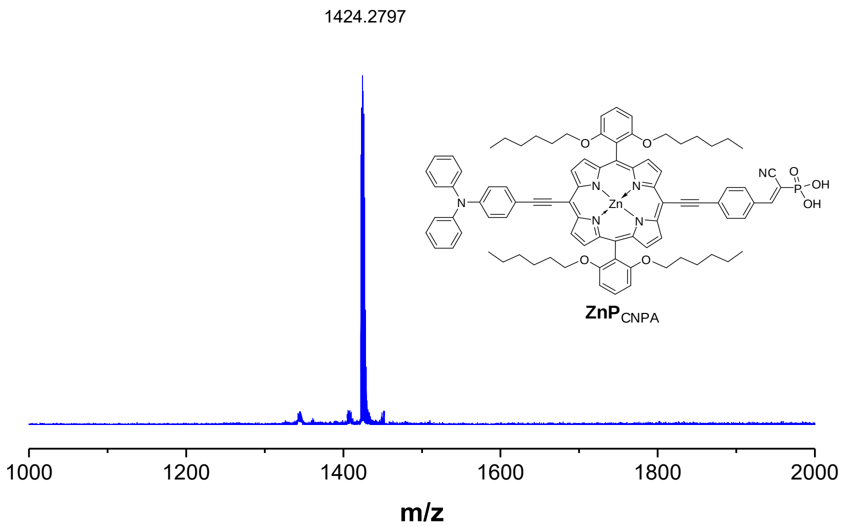

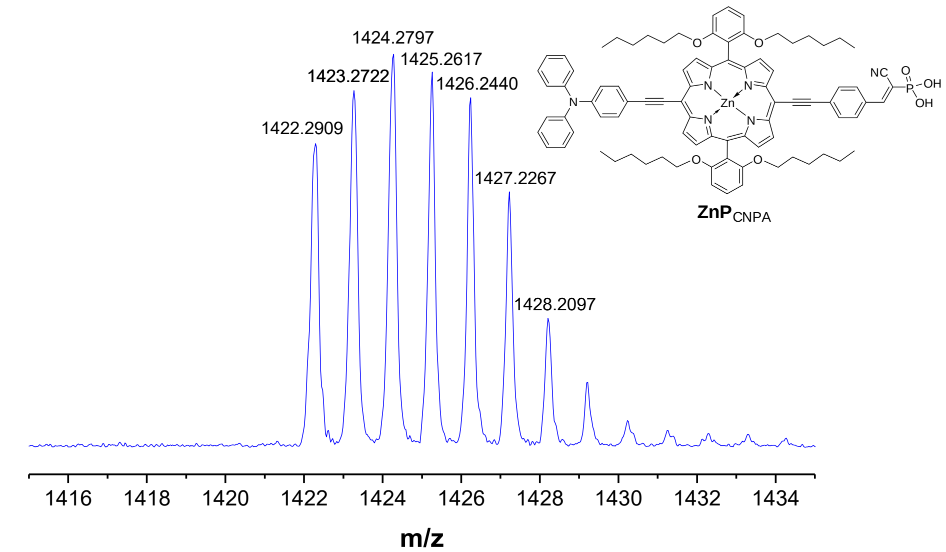

Figure S17. MALDI-TOF mass spectrum of **ZnP$_{CNPA}$**.

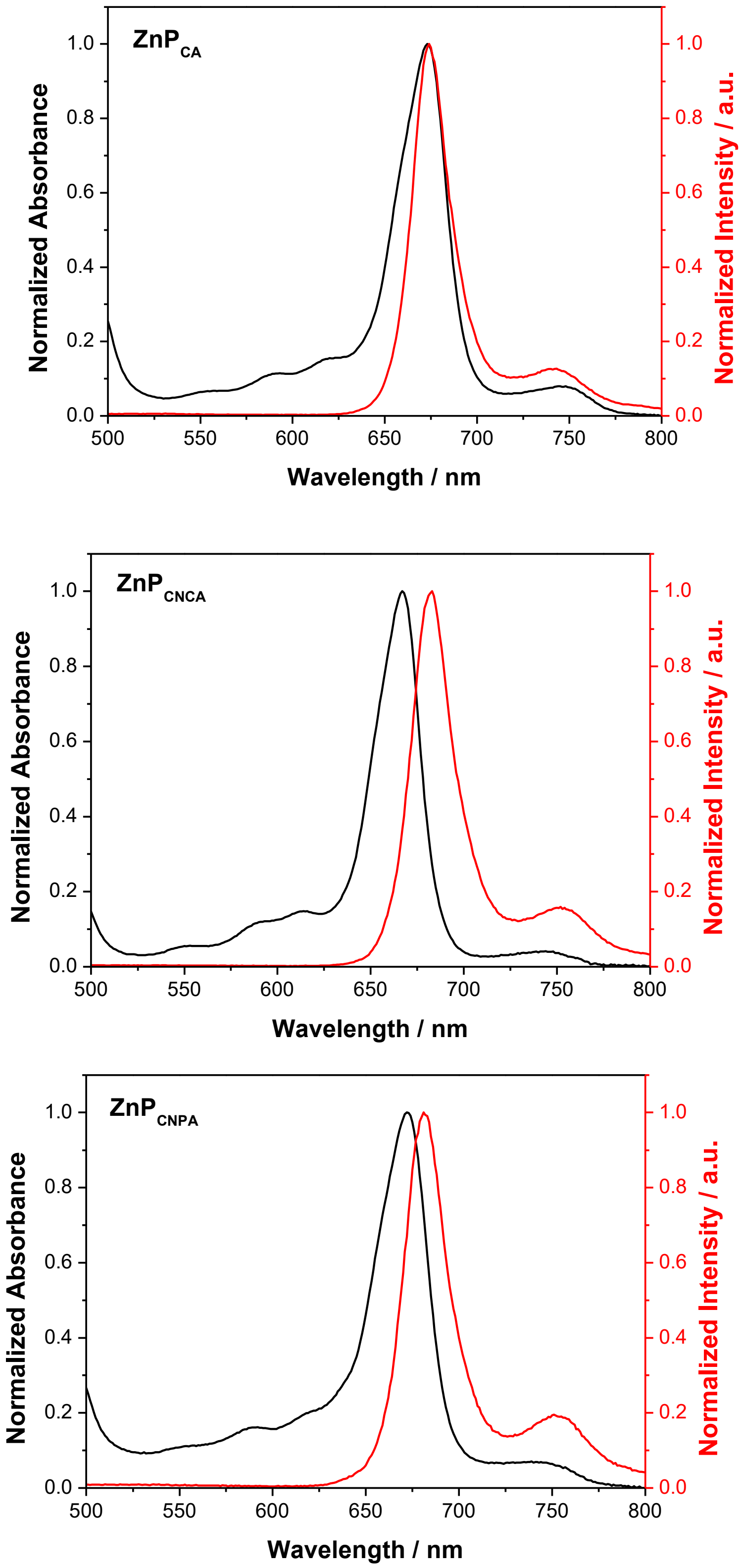

Figure S18. UV-Vis absorption (black) and photoluminescence spectra (red) of 1.65 μM **ZnPs** (in DMF): photoluminescence spectra were measured by excitation of 667 nm (**ZnP$_{CA}$**), 674 nm (**ZnP$_{CNCA}$**), and 674 nm (**ZnP$_{CNPA}$**).

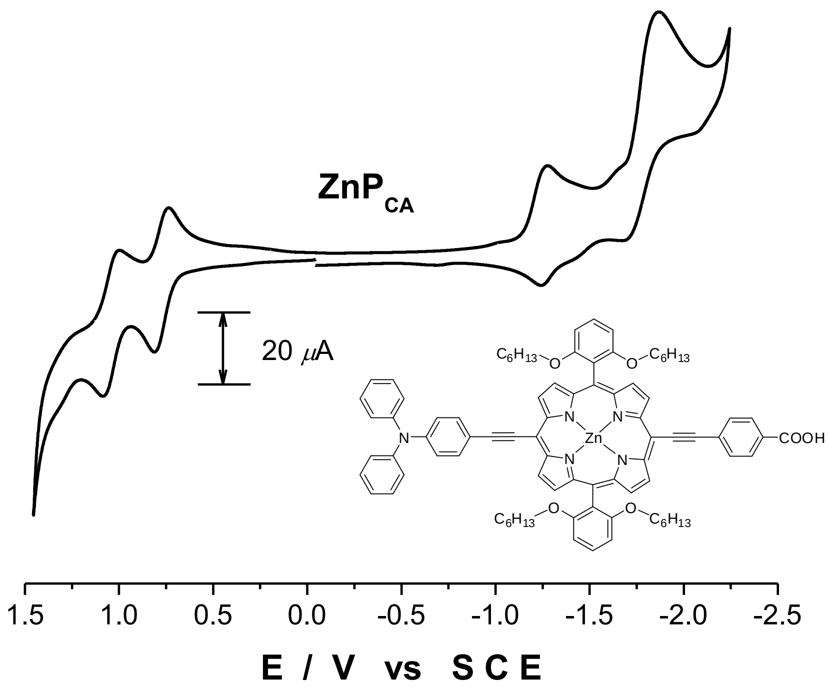

Figure S19. Cyclic voltammogram of **ZnP$_{CA}$**.

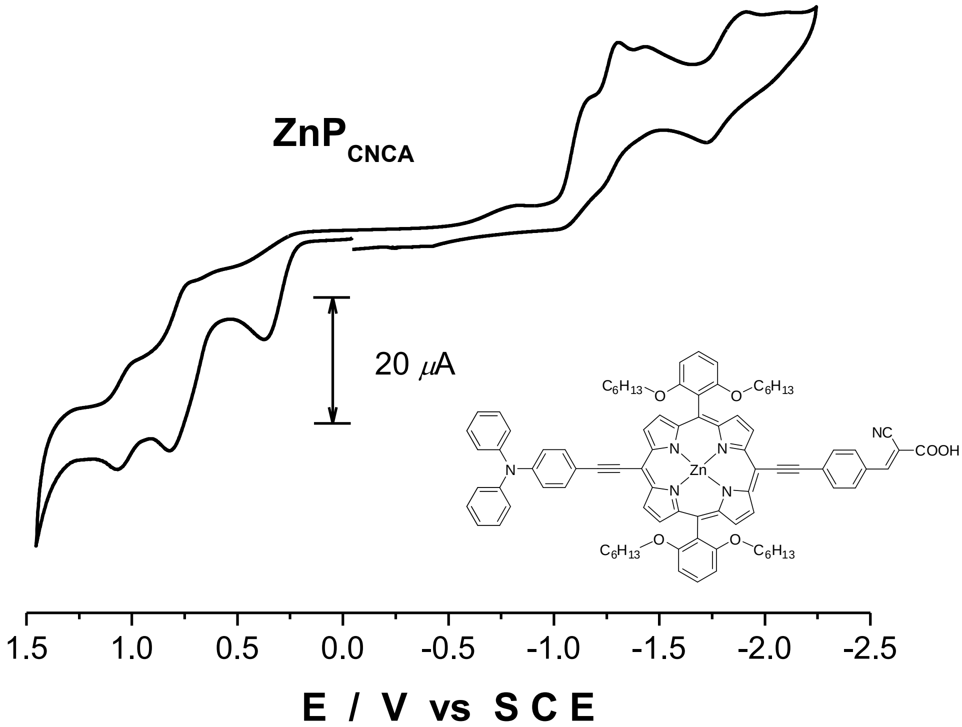

Figure S20. Cyclic voltammogram of **ZnP$_{CNCA}$**.

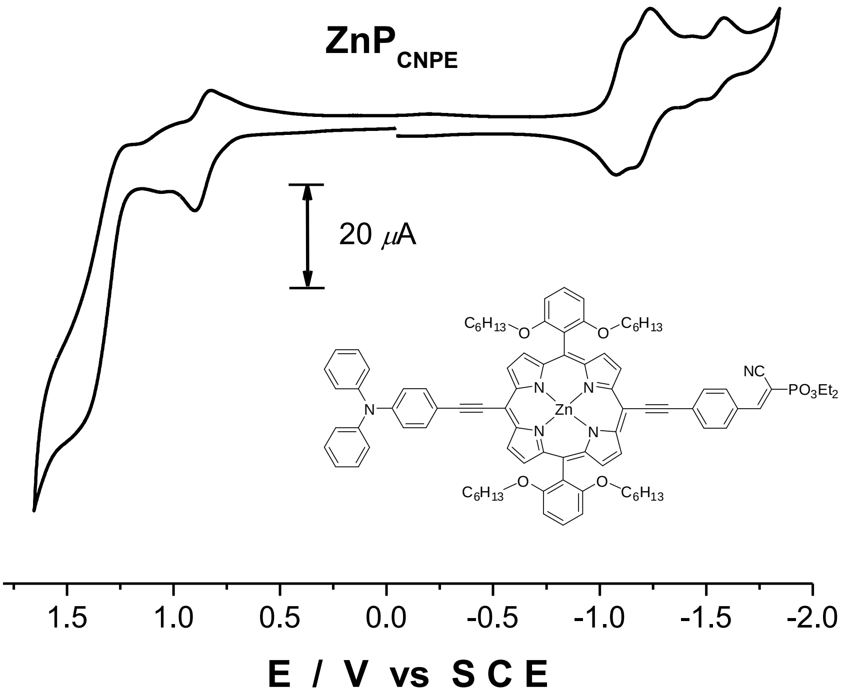

Figure S21. Cyclic voltammogram of **ZnP$_{CNPE}$**.

Theoretical calculation. All the calculations were performed on the platform of the Gaussian 09 package.[4] The ground-state geometries were optimized by using the B3LYP density functional theory (DFT),[5–8] 6-31G(d,p) basis set,[9] and LANL2DZ basis set[10] for zinc metal. Time-dependent DFT (TDDFT) calculations were then performed with the same functional and basis set to estimate the energies and oscillator strengths of the derivatives. The isodensity plots (contour = 0.03 a.u.) of the frontier orbitals were visualized by the Chem3D Ultra program.

[4] Frisch, M. J.; Trucks, G. W.; Schlegel, H. B.; Scuseria, G. E.; Robb, M. A.; Cheeseman, J. R.; Scalmani, G.; Barone, V.; Mennucci, B.; Petersson, G. A.; Nakatsuji, H.; Caricato, M.; Li, X.; Hratchian, H. P.; Izmaylov, A. F.; Bloino, J.; Zheng, G.; Sonnenberg, J. L.; Hada, M.; Ehara, M.; Toyota, K.; Fukuda, R.; Hasegawa, J.; Ishida, M.; Nakajima, T.; Honda, Y.; Kitao, O.; Nakai, H.; Vreven, T.; Montgomery, Jr., J. A.; Peralta, J. E.; Ogliaro, F.; Bearpark, M.; Heyd, J. J.; Brothers, E.; Kudin, K. N.; Staroverov, V. N.; Kobayashi, R.; Normand, J.; Raghavachari, K.; Rendell, A.; Burant, J. C.; Iyengar, S. S.; Tomasi, J.; Cossi, M.; Rega, N.; Millam, J. M.; Klene, M.; Knox, J. E.; Cross, J. B.; Bakken, V.; Adamo, C.; Jaramillo, J.; Gomperts, R.; Stratmann, R. E.; Yazyev, O.; Austin, A. J.; Cammi, R.; Pomelli, C.; Ochterski, J. W.; Martin, R. L.; Morokuma, K.; Zakrzewski, V. G.; Voth, G. A.; Salvador, P.; Dannenberg, J. J.; Dapprich, S.; Daniels, A. D.; Farkas, Ö.; Foresman, J. B.; Ortiz, J. V.; Cioslowski, J.; Fox, D. J. Gaussian 09, Revision D.01; Gaussian Inc.: Wallingford, CT, **2009**.

[5] Hohenberg, P.; Kohn, W. *Phys. Rev.* **1964**, *136*, B864–B871.

[6] Kohn, W.; Sham, L. J. *Phys. Rev.* **1965**, *140*, A1133–A1138.

[7] Parr, R. G.; Yang, W. *Density-Functional Theory of Atoms and Molecules*; Oxford University Press: New York, **1989**.

[8] Petersson, G. A.; Bennett, A.; Tensfeldt, T. G.; Al-Laham, M. A.; Shirley, W. A.; Mantzaris, J. *J. Chem. Phys.* **1988**, *89*, 2193–2218.

[9] Petersson, G. A.; Al-Laham, M. A. *J. Chem. Phys.* **1991**, *94*, 6081–6090.

[10] Hay, P. J.; Wadt, W. R. *J. Chem. Phys.* **1985**, *82*, 299–310.

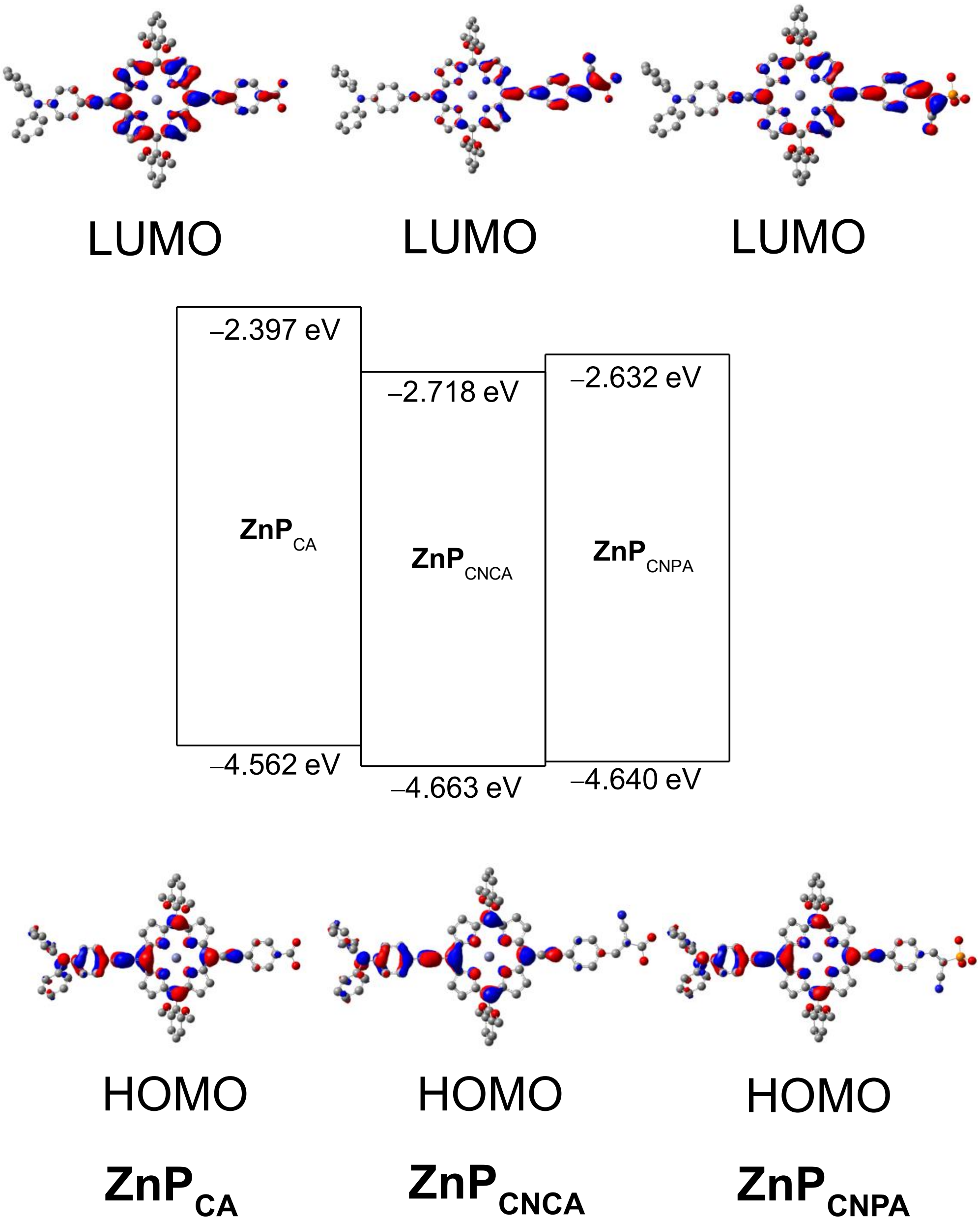

Figure S22. Calculated energetics of **ZnPs** antenna.

Chart S1. DFT calculation results of **ZnP$_{CA}$**.

No.	Energy (cm^{-1})	Wavelength (nm)	Osc. Strength	Symmetry	Major contribs
1	15596.45072	641.171519054	1.0768	Singlet	H-1->L+1 (-10%), HOMO->LUMO (90%)
2	16732.0872	597.654069123	0.0001	Singlet	H-1->LUMO (44%), HOMO->L+1 (54%)
3	19723.61824	507.006365583	0.122	Singlet	H-2->LUMO (83%), H-1->L+1 (13%)
4	21692.4312	460.990283099	0.2552	Singlet	H-2->L+1 (31%), H-1->LUMO (-33%), HOMO->L+1 (35%)
5	23339.42672	428.459538444	0.2292	Singlet	HOMO->L+2 (81%)
6	23899.98592	418.410288335	1.8266	Singlet	H-5->LUMO (-10%), H-1->L+1 (51%), HOMO->L+2 (-11%)
7	24291.16752	411.672266957	0.4016	Singlet	H-2->L+1 (61%), H-1->LUMO (19%)
8	24810.59216	403.053660933	0.0049	Singlet	H-3->LUMO (98%)
9	24876.73008	401.982092013	0.0044	Singlet	H-4->LUMO (98%)
10	25722.81152	388.759991972	0.0	Singlet	H-6->LUMO (99%)
11	25823.63152	387.242204577	0.0005	Singlet	H-7->LUMO (99%)
12	25839.76272	387.000457719	0.0697	Singlet	H-5->LUMO (78%)
13	26526.14528	376.98655023	0.162	Singlet	H-1->L+2 (87%)
14	27026.21248	370.011151485	0.0063	Singlet	H-8->LUMO (93%)
15	27156.8752	368.23087805	0.0222	Singlet	H-9->LUMO (85%)
16	27494.82384	363.704821613	0.0005	Singlet	H-3->L+1 (94%)
17	27554.50928	362.917005648	0.0005	Singlet	H-4->L+1 (95%)
18	27892.45792	358.519856109	0.0	Singlet	H-6->L+1 (96%)
19	27960.20896	357.651118213	0.0	Singlet	H-2->L+2 (-30%), HOMO->L+3 (55%)
20	27971.5008	357.506737715	0.0	Singlet	H-7->L+1 (96%)
21	28318.3216	353.128272969	0.02	Singlet	H-10->LUMO (46%), H-2->L+2 (22%), HOMO->L+3 (20%)
22	28728.05408	348.091798078	0.0435	Singlet	H-9->LUMO (10%), H-5->L+1 (78%)
23	29078.90768	343.891872076	0.0148	Singlet	H-10->LUMO (-33%), H-2->L+2 (35%)
24	29542.67968	338.493329255	0.0085	Singlet	H-2->L+4 (12%), HOMO->L+4 (82%)
25	29633.82096	337.45226488	0.0	Singlet	H-14->LUMO (98%)
26	29829.00848	335.244130113	0.0952	Singlet	H-12->LUMO (42%), H-11->LUMO (11%), H-8->L+1 (-41%)
27	30719.45072	325.526653818	0.0469	Singlet	H-12->LUMO (39%), H-8->L+1 (53%)
28	30734.77536	325.364343252	0.0917	Singlet	HOMO->L+5 (88%)
29	31102.56672	321.51687319	0.0291	Singlet	H-9->L+1 (72%), HOMO->L+6 (-16%)
30	31164.67184	320.876152694	0.0726	Singlet	H-1->L+3 (83%)
31	31232.42288	320.180091004	0.0622	Singlet	H-11->LUMO (-14%), H-9->L+1 (19%), HOMO->L+6 (57%)
32	31663.12592	315.824787018	0.0072	Singlet	H-11->LUMO (38%), H-2->L+3 (11%), HOMO->L+6 (15%)
33	31867.99216	313.794479106	0.0002	Singlet	H-10->L+1 (83%)
34	32268.85248	309.896362326	0.0	Singlet	H-14->L+1 (98%)
35	32319.66576	309.409140375	0.0	Singlet	H-19->LUMO (93%)
36	32648.74224	306.290512709	0.0001	Singlet	H-16->LUMO (-16%), HOMO->L+7 (76%)
37	32661.6472	306.169494109	0.0002	Singlet	H-21->LUMO (90%)
38	32706.008	305.754221059	0.0189	Singlet	H-2->L+3 (78%)
39	32909.26112	303.865831674	0.0017	Singlet	H-13->LUMO (76%), HOMO->L+11 (12%)
40	33291.57056	300.376336466	0.0	Singlet	HOMO->L+8 (97%)

Chart S2. DFT calculation results of **ZnP$_{\mathbf{CNCA}}$.**

No.	Energy (cm^{-1})	Wavelength (nm)	Osc. Strength	Symmetry	Major contribs
1	14268.85296	700.827181276	1.4295	Singlet	HOMO->LUMO (96%)
2	16208.62976	616.955297768	0.0035	Singlet	H-1->LUMO (61%), HOMO->L+2 (35%)
3	17949.9928	557.103287529	0.0231	Singlet	H-2->LUMO (34%), H-1->L+2 (12%), HOMO->L+1 (50%)
4	18871.08432	529.911256313	0.0039	Singlet	H-2->LUMO (60%), HOMO->L+1 (-38%)
5	19257.42656	519.280183613	0.0788	Singlet	H-1->LUMO (-30%), H-1->L+1 (-32%), HOMO->L+2 (37%)
6	22082.80624	452.840997259	1.2337	Singlet	H-2->L+1 (54%), H-1->L+2 (-32%)
7	22198.14432	450.488106386	0.0828	Singlet	H-2->L+2 (52%), H-1->L+1 (32%), HOMO->L+2 (14%)
8	23126.49488	432.404480311	0.0037	Singlet	H-3->LUMO (97%)
9	23416.85648	427.042801776	0.0332	Singlet	H-4->LUMO (95%)
10	23602.36528	423.686350133	0.6174	Singlet	H-5->LUMO (58%), H-2->L+1 (-21%), H-1->L+2 (-13%)
11	24238.74112	412.562680153	0.0001	Singlet	H-6->LUMO (96%)
12	24512.16496	407.960700996	0.0002	Singlet	H-7->LUMO (96%)
13	24925.12368	401.201620035	0.6595	Singlet	H-2->L+2 (40%), H-1->L+1 (-32%), HOMO->L+2 (-12%)
14	25311.46592	395.077868331	0.3799	Singlet	H-10->LUMO (15%), H-5->LUMO (28%), H-2->L+1 (14%), H-1->L+2 (17%), HOMO->L+3 (-16%)
15	25989.78288	384.76658486	0.0399	Singlet	H-9->LUMO (-34%), H-8->LUMO (57%)
16	26276.91824	380.562130942	0.0016	Singlet	H-9->LUMO (55%), H-8->LUMO (32%)
17	26889.09728	371.897944206	0.007	Singlet	H-10->LUMO (22%), HOMO->L+3 (69%)
18	27067.34704	369.448841263	0.0008	Singlet	H-3->L+2 (89%)
19	27332.70528	365.862065154	0.0004	Singlet	H-4->L+2 (88%)
20	27555.31584	362.906382858	0.0001	Singlet	H-6->L+2 (91%)
21	27560.96176	362.832040735	0.0081	Singlet	H-11->LUMO (42%), H-10->LUMO (27%)
22	27791.63792	359.82046214	0.0	Singlet	H-7->L+2 (91%)
23	27946.49744	357.826594244	0.0006	Singlet	H-3->L+1 (89%)
24	28247.34432	354.015580605	0.0029	Singlet	H-4->L+1 (88%)
25	28412.68912	351.955422374	0.0415	Singlet	H-5->L+2 (82%)
26	28445.75808	351.546264715	0.0206	Singlet	H-11->LUMO (-13%), H-5->L+1 (64%)
27	28976.47456	345.107545064	0.0001	Singlet	H-15->LUMO (87%), H-15->L+1 (-11%)
28	29099.87824	343.644049557	0.2751	Singlet	H-12->LUMO (65%), H-5->L+1 (14%)
29	29197.472	342.495405082	0.0001	Singlet	H-6->L+1 (90%)
30	29482.18768	339.187855004	0.0001	Singlet	H-7->L+1 (91%)
31	29728.18848	336.381075044	0.0087	Singlet	H-2->L+4 (12%), HOMO->L+4 (79%)
32	30157.2784	331.59490944	0.0283	Singlet	H-1->L+3 (86%)
33	30200.02608	331.125541862	0.0018	Singlet	H-11->LUMO (27%), H-10->LUMO (-14%)
34	30381.50208	329.147649569	0.0005	Singlet	H-12->LUMO (13%), H-8->L+2 (76%)
35	31009.00576	322.486959995	0.1005	Singlet	HOMO->L+6 (76%)
36	31021.10416	322.361188319	0.0463	Singlet	H-9->L+2 (66%), HOMO->L+6 (-10%)
37	31085.62896	321.692059468	0.0048	Singlet	H-9->L+1 (-10%), H-8->L+1 (77%)
38	31204.99984	320.461466152	0.1043	Singlet	H-9->L+2 (13%), HOMO->L+5 (57%)
39	31355.82656	318.919993414	0.006	Singlet	H-10->L+2 (17%), H-9->L+1 (62%)
40	31475.19744	317.710477244	0.001	Singlet	H-2->L+3 (72%), HOMO->L+5 (-12%)

Chart S3. DFT calculation results of **ZnP$_{\mathbf{CNPA}}$**.

No.	Energy (cm^{-1})	Wavelength (nm)	Osc. Strength	Symmetry	Major contribs
1	14625.35248	683.744204707	1.4307	Singlet	HOMO->LUMO (94%)
2	16394.94512	609.944097208	0.0017	Singlet	H-1->LUMO (55%), HOMO->L+2 (-42%)
3	18450.06	542.003657441	0.0001	Singlet	H-2->LUMO (45%), H-1->L+2 (-13%), HOMO->L+1 (38%)
4	19360.66624	516.511150806	0.0059	Singlet	H-2->LUMO (-47%), HOMO->L+1 (51%)
5	19915.57952	502.119458284	0.1195	Singlet	H-1->LUMO (34%), H-1->L+1 (29%), HOMO->L+2 (35%)
6	22394.1384	446.545422797	0.0482	Singlet	H-2->L+2 (54%), H-1->L+1 (-35%), HOMO->L+2 (10%)
7	22582.87344	442.813445621	1.6338	Singlet	H-2->L+1 (39%), H-1->L+2 (40%)
8	23554.77824	424.542311463	0.001	Singlet	H-3->LUMO (98%)
9	23816.91024	419.869743776	0.0132	Singlet	H-4->LUMO (96%)
10	24000.80592	416.65267547	0.3252	Singlet	H-5->LUMO (53%), H-2->L+1 (-33%)
11	24618.63088	406.196431018	0.0001	Singlet	H-6->LUMO (97%)
12	24867.85792	402.125508042	0.0004	Singlet	H-7->LUMO (97%)
13	24987.2288	400.20444364	0.658	Singlet	H-2->L+2 (37%), H-1->LUMO (-10%), H-1->L+1 (33%), HOMO->L+2 (-12%)
14	25524.39776	391.782015546	0.2897	Singlet	H-10->LUMO (13%), H-5->LUMO (31%), H-2->L+1 (16%), H-1->L+2 (-14%), HOMO->L+3 (-18%)
15	26280.95104	380.503733856	0.0305	Singlet	H-9->LUMO (-26%), H-8->LUMO (67%)
16	26509.20752	377.227421546	0.0036	Singlet	H-9->LUMO (64%), H-8->LUMO (24%)
17	27059.28144	369.558963425	0.007	Singlet	H-10->LUMO (18%), HOMO->L+3 (68%)
18	27158.48832	368.209006414	0.0012	Singlet	H-3->L+2 (93%)
19	27396.42352	365.011147995	0.0005	Singlet	H-4->L+2 (92%)
20	27622.26032	362.026853855	0.0	Singlet	H-6->L+2 (94%)
21	27823.90032	359.403242715	0.0061	Singlet	H-11->LUMO (36%), H-10->LUMO (36%)
22	27835.99872	359.247034769	0.0	Singlet	H-7->L+2 (93%)
23	28458.66304	351.386851376	0.0465	Singlet	H-5->L+2 (83%)
24	28728.86064	348.082025435	0.0005	Singlet	H-3->L+1 (94%)
25	28952.27776	345.395967906	0.0002	Singlet	H-12->LUMO (14%), H-11->LUMO (17%), H-5->L+1 (-23%), H-4->L+1 (32%)
26	29046.64528	344.273836225	0.0023	Singlet	H-5->L+1 (17%), H-4->L+1 (62%)
27	29153.1112	343.016562843	0.0	Singlet	H-15->LUMO (91%)
28	29440.24656	339.671068298	0.3167	Singlet	H-12->LUMO (48%), H-5->L+1 (34%)
29	29694.31296	336.764821381	0.0088	Singlet	H-2->L+4 (12%), HOMO->L+4 (80%)
30	30008.87136	333.234791807	0.0001	Singlet	H-6->L+1 (94%)
31	30254.0656	330.534088615	0.0304	Singlet	H-1->L+3 (88%)
32	30279.87552	330.252348409	0.0001	Singlet	H-7->L+1 (93%)
33	30392.79392	329.025361285	0.0043	Singlet	H-8->L+2 (65%)
34	30587.17488	326.934410884	0.0025	Singlet	H-12->LUMO (-13%), H-11->LUMO (19%), H-10->LUMO (-10%), H-8->L+2 (15%), H-5->L+1 (12%)
35	30953.35312	323.066776037	0.098	Singlet	HOMO->L+6 (84%)
36	31076.7568	321.783899921	0.0376	Singlet	H-9->L+2 (80%)
37	31250.1672	319.998287881	0.0991	Singlet	H-9->L+2 (-10%), HOMO->L+5 (57%)
38	31612.31264	316.33244027	0.0028	Singlet	H-10->L+2 (-15%), H-2->L+3 (53%)
39	31626.02416	316.195293768	0.0098	Singlet	H-11->L+2 (15%), H-10->L+2 (38%), H-2->L+3 (21%)
40	31692.96864	315.527400213	0.0007	Singlet	H-20->LUMO (18%), HOMO->L+7 (68%)

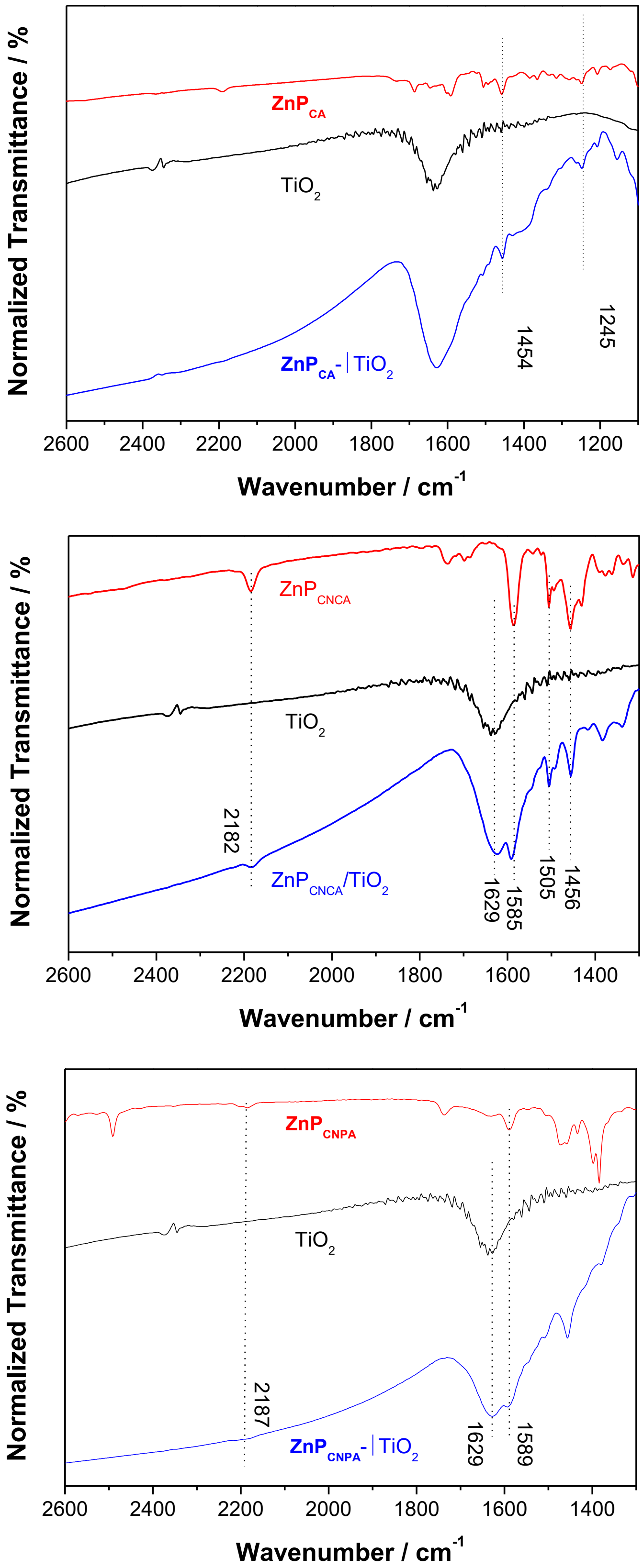

Figure S23. IR spectra comparison of **ZnPs** (**ZnP**$_{CA}$, **ZnP**$_{CNCA}$, and **ZnP**$_{CNPA}$), bare TiO_2 particles, and porphyrin-sensitized TiO_2 powders (**ZnP**$_{CA}$-|TiO_2, **ZnP**$_{CNCA}$-|TiO_2, and **ZnP**$_{CNPA}$-|TiO_2) in KBr disc.

TOF-SIMS characterization: TOF-SIMS experiments were performed with a TOF-SIMS 5 (ION-TOF GmbH, Münster, Germany) in KBSI Busan Center by using a pulsed 30 keV Bi^+ primary beam with a current 0.60 pA. The analyzed area used in this work is a square of 200 μm × 200 μm and the data acquisition time is around 40 s. A negative ion spectra were internally calibrated using H^-, C^-, C_2^-, C_3^-, and C_4^- peaks and a positive ion spectra were internally calibrated using H^+, CH_3^+, $C_2H_5^+$, $C_3H_7^+$, $C_4H_9^+$ normalized to the respective secondary total ion yields. The chemical images of the analyzed area are recorded with 128 × 128 pixel resolution during the data acquisition.

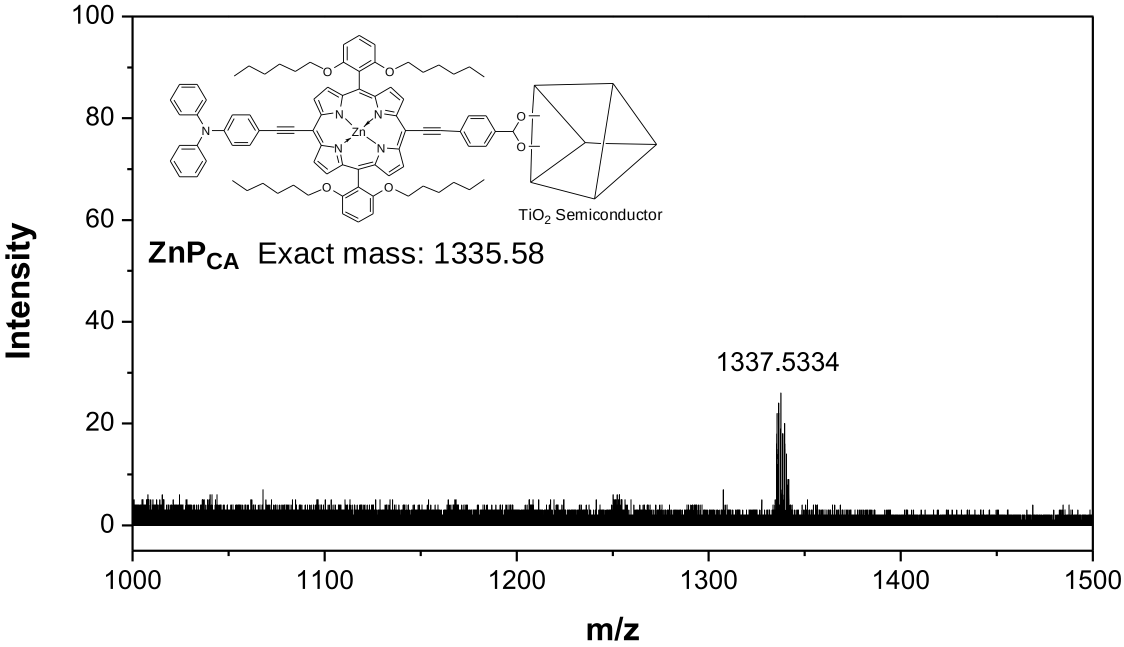

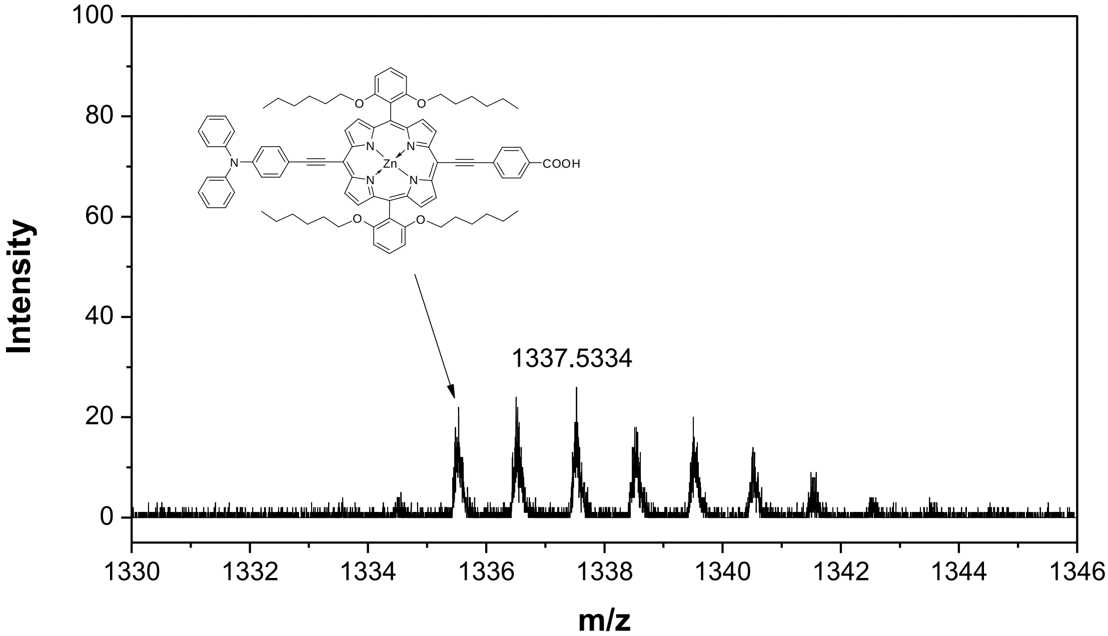

Figure S24. TOF-SIMS mass spectra of **ZnP$_{CA}$-**|TiO_2|**-ReC** particles.

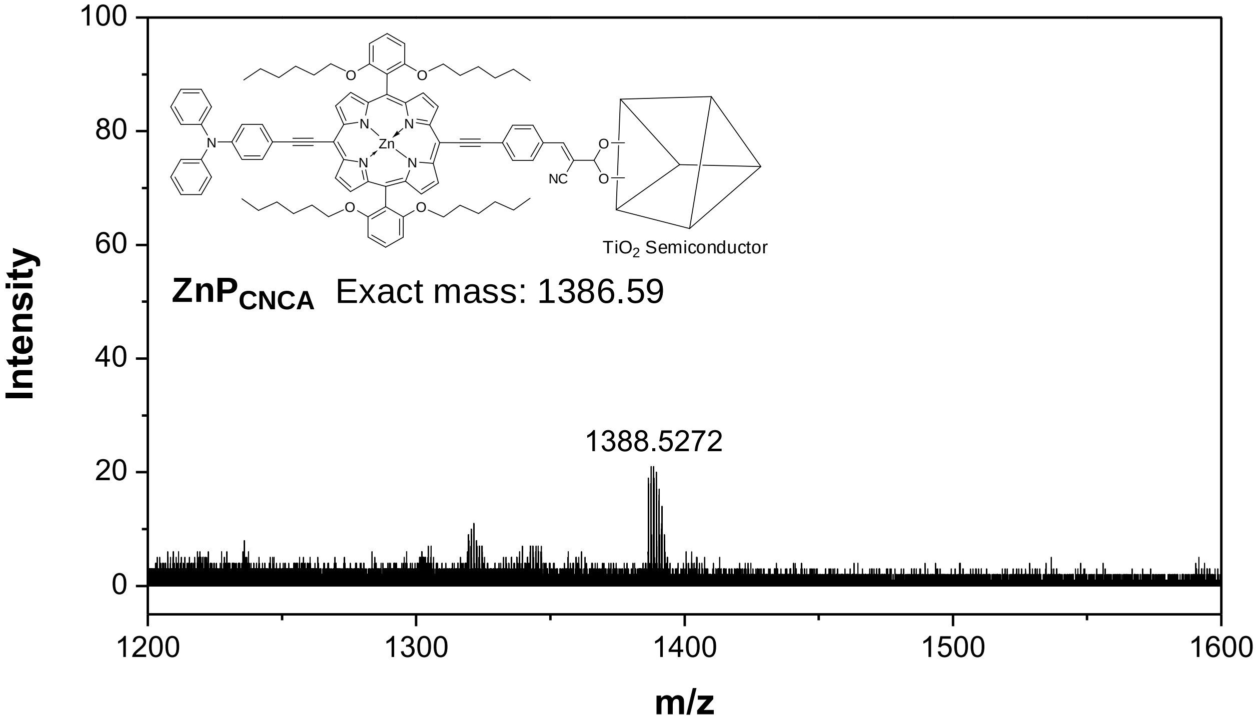

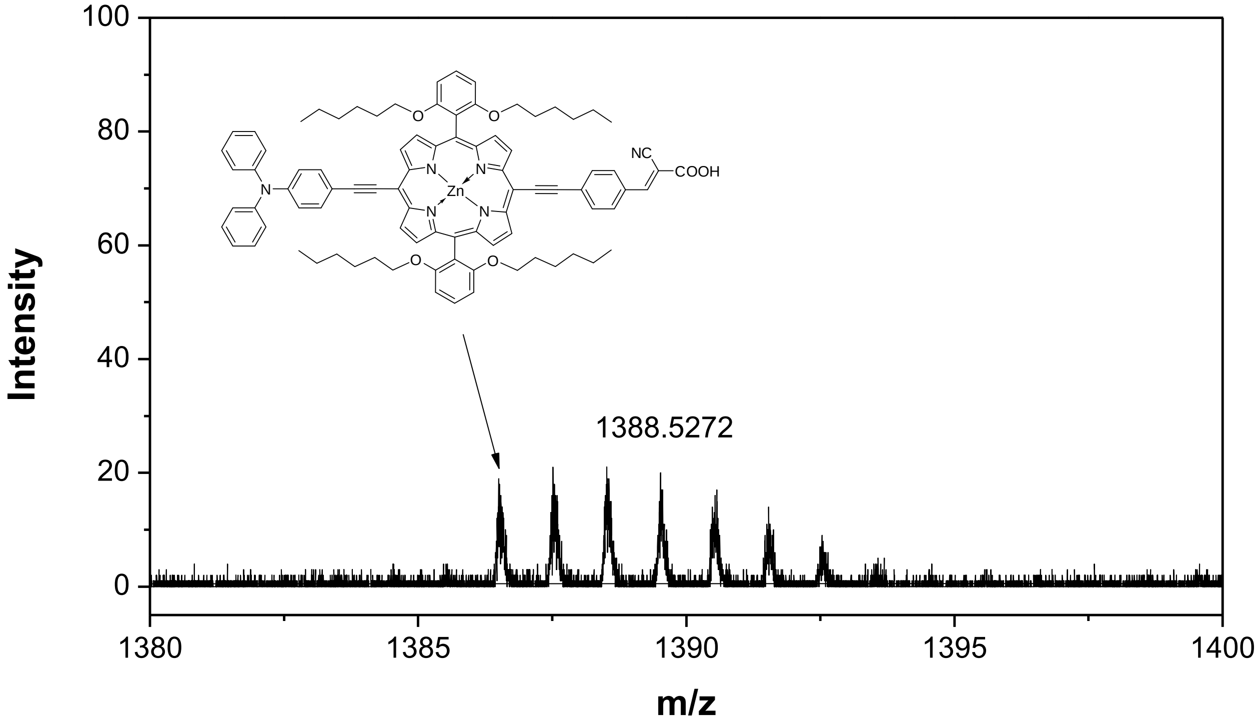

Figure S25. TOF-SIMS mass spectra of **ZnP$_{\mathbf{CNCA}}$-**|TiO$_2$|**-ReC** particles.

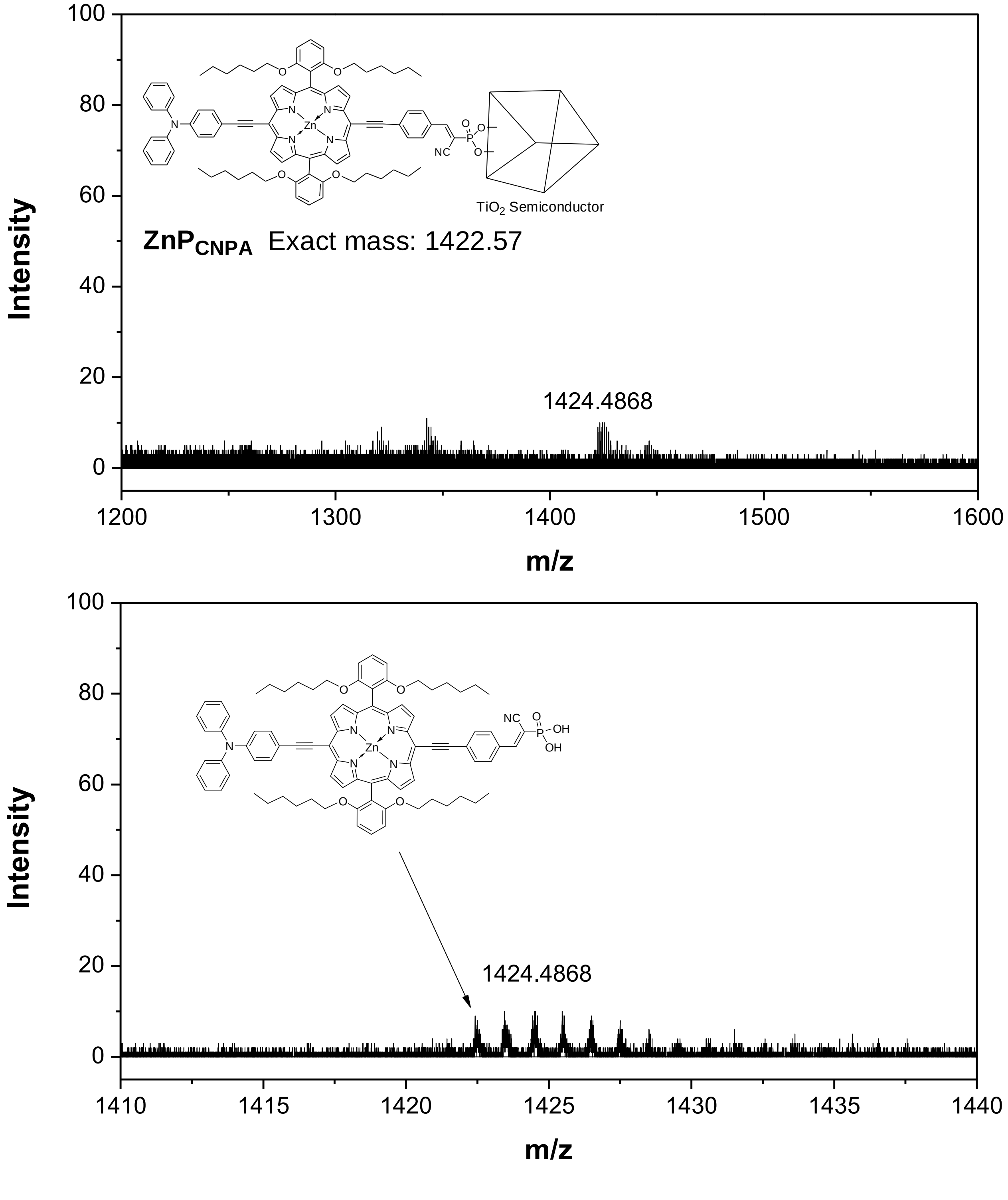

Figure S26. TOF-SIMS mass spectra of **ZnP$_{CNPA}$**-|TiO_2|-**ReC** particles.

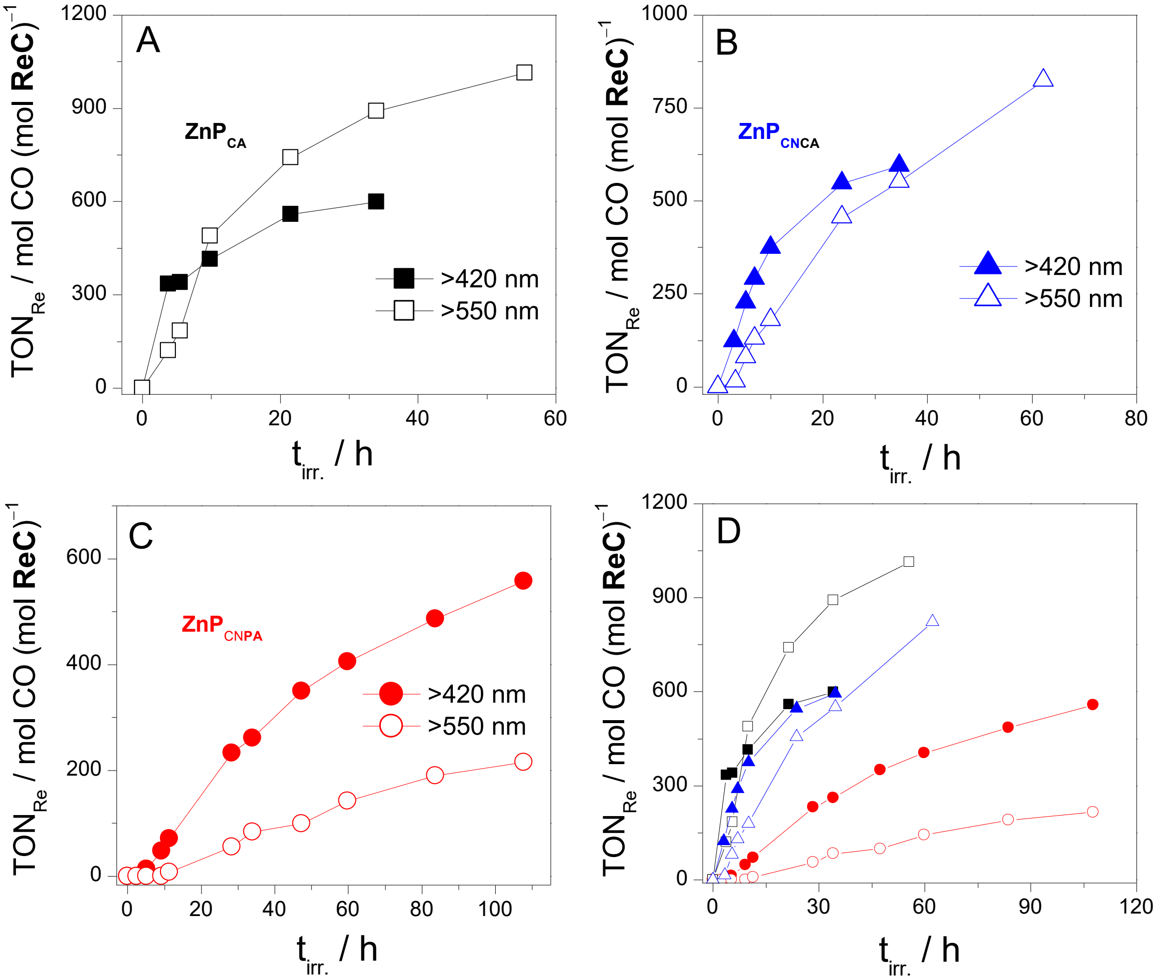

Figure S27. Time courses for CO formation for (A) **ZnP$_{CA}$**-|TiO_2|-**ReC** (-■- at λ >550 nm; -□- at λ >420 nm), (B) **ZnP$_{CNCA}$**-|TiO_2|-**ReC** (-▲- at λ >550 nm; -△- at λ >420 nm), (C) **ZnP$_{CNPA}$**-|TiO_2|-**ReC** (-●- at λ >550 nm; -○- at λ >420 nm), and (D) overlapped plots in the presence of 0.1 M BIH under light at an intensity of 109 mW/cm^2.

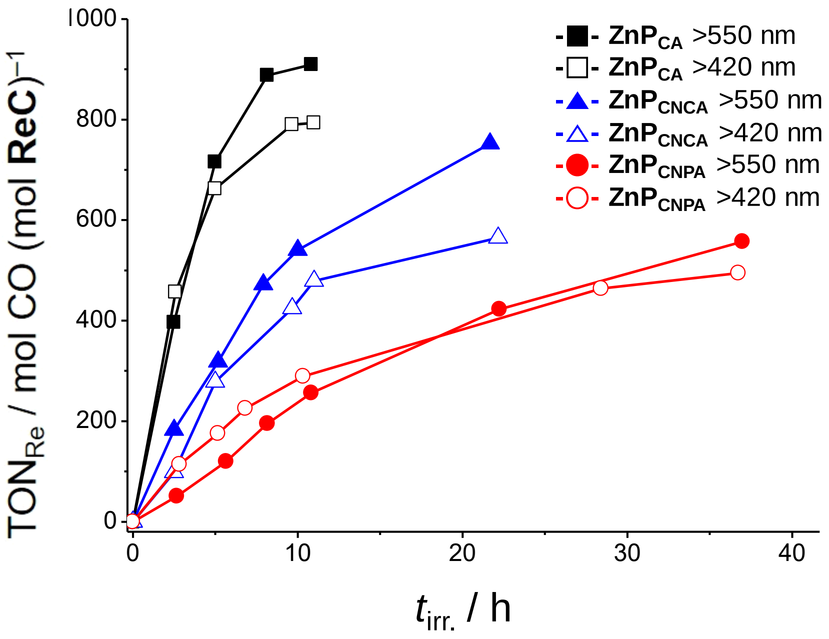

Figure S28. Time courses for CO formation for **ZnP$_{CA}$**-|TiO_2|-**ReC** (-■- at λ >550 nm; -□- at λ >420 nm), **ZnP$_{CNCA}$**-|TiO_2|-**ReC** (-▲- at λ >550 nm; -△- at λ >420 nm), and **ZnP$_{CNPA}$**-|TiO_2|-**ReC** (-●- at λ >550 nm; -○- at λ >420 nm) in the presence of 0.1 M BIH under light at an intensity of 414 mW/cm^2.

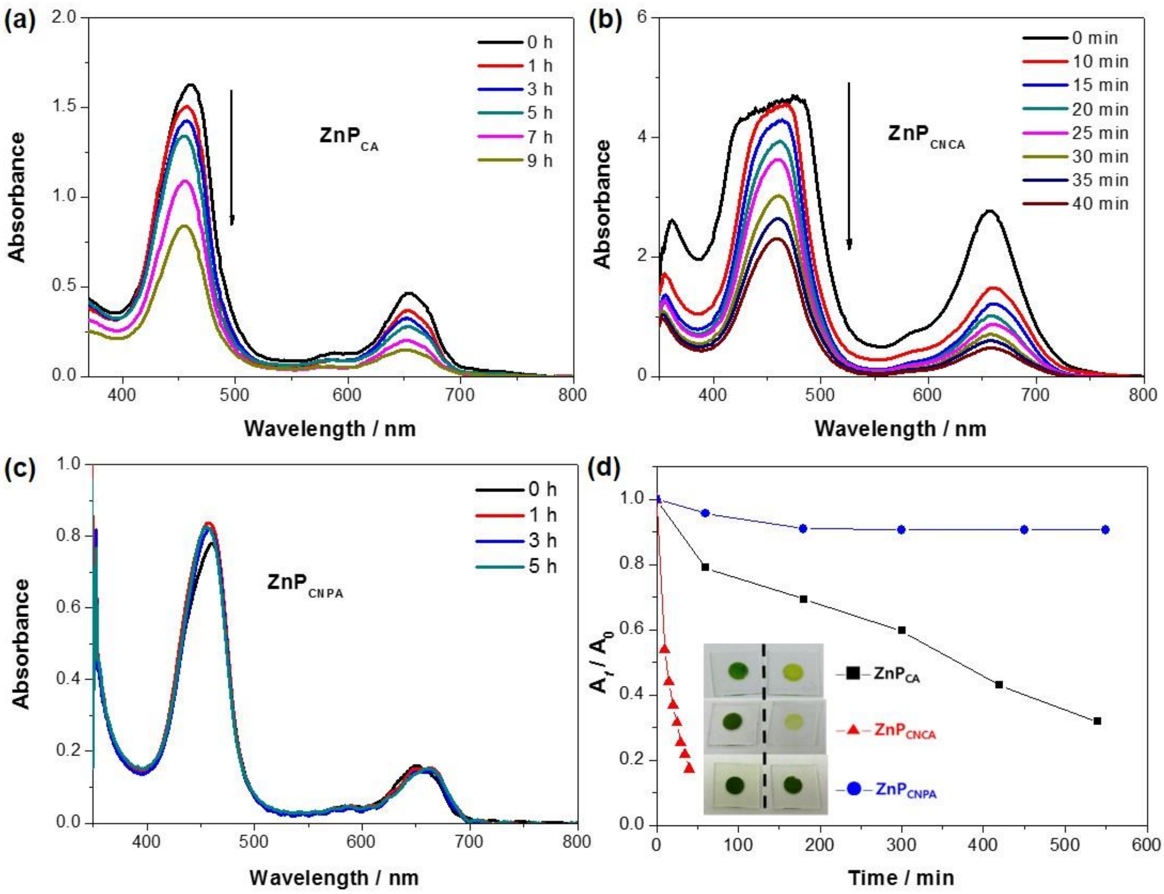

Figure S29. Absorption spectra of (a) **ZnP$_{CA}$-**|TiO_2, (b) **ZnP$_{CNCA}$-**|TiO_2, and (c) **ZnP$_{CNPA}$-**|TiO_2 film after soaking in DMF solvent for various time scale. (d) Relative A_t/A_0 absorbance of **ZnP$_{CA}$-**|TiO_2, **ZnP$_{CNCA}$-**|TiO_2, and **ZnP$_{CNPA}$-**|TiO_2 film at 650 nm after soaking in DMF solvent and photos of films before/after 10 h soaking.

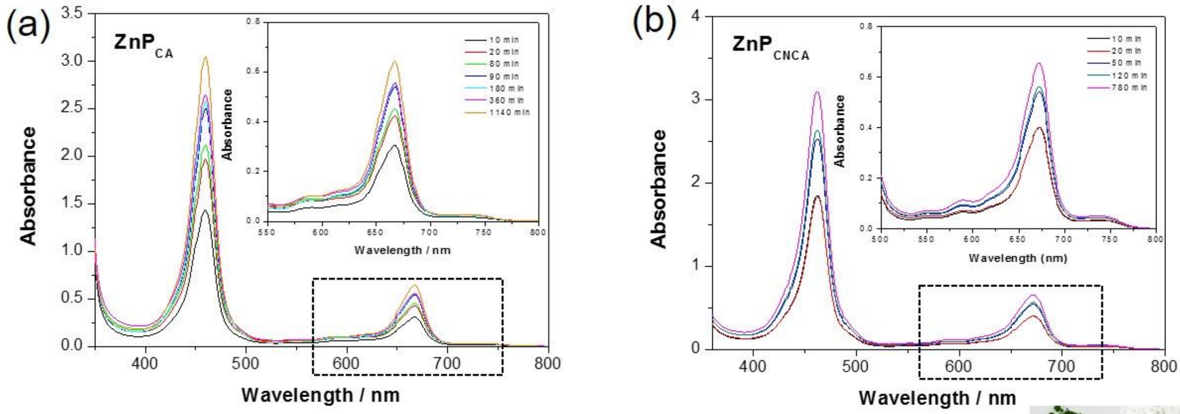

(c)

ZnP$_{CA}$	Amount of desorption	ZnP$_{CNCA}$	Amount of desorption
10 min	1.19×10^{-7} mol	10 min	1.68×10^{-7} mol
20 min	1.66×10^{-7} mol	20 min	1.68×10^{-7} mol
80 min	1.78×10^{-7} mol	50 min	2.26×10^{-7} mol
90 min	2.14×10^{-7} mol	120 min	2.35×10^{-7} mol
180 min	2.18×10^{-7} mol	780 min	2.72×10^{-7} mol
360 min	2.22×10^{-7} mol		
1140 min	2.53×10^{-7} mol		

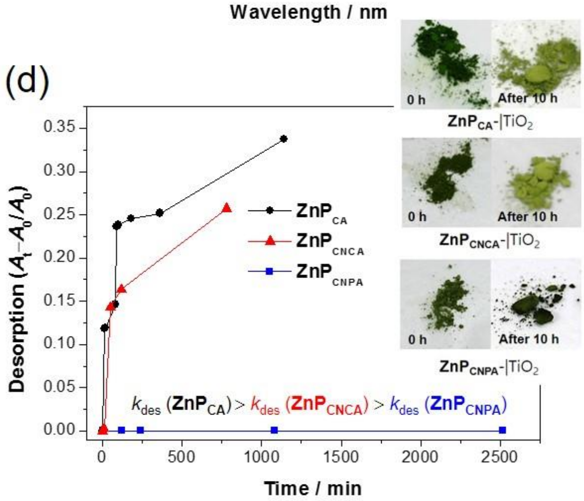

Figure S30. Absorbance comparison of (a) **ZnP$_{CA}$** and (b) **ZnP$_{CNCA}$** (present in supernatant) desorbed with different exposing periods, (c) the desorption amount of **ZnP$_{CA}$** and **ZnP$_{CNCA}$** desorbed from TiO_2 nanoparticles, and (d) the time desorption kinetics (A_t–A_0/A_0) of **ZnP$_{CA}$**, **ZnP$_{CNCA}$**, and **ZnP$_{CNPA}$** in DMF solvent for 20 h and photo images of **ZnPs-**|TiO_2 particles before/after 10 h soaking in DMF solvent.

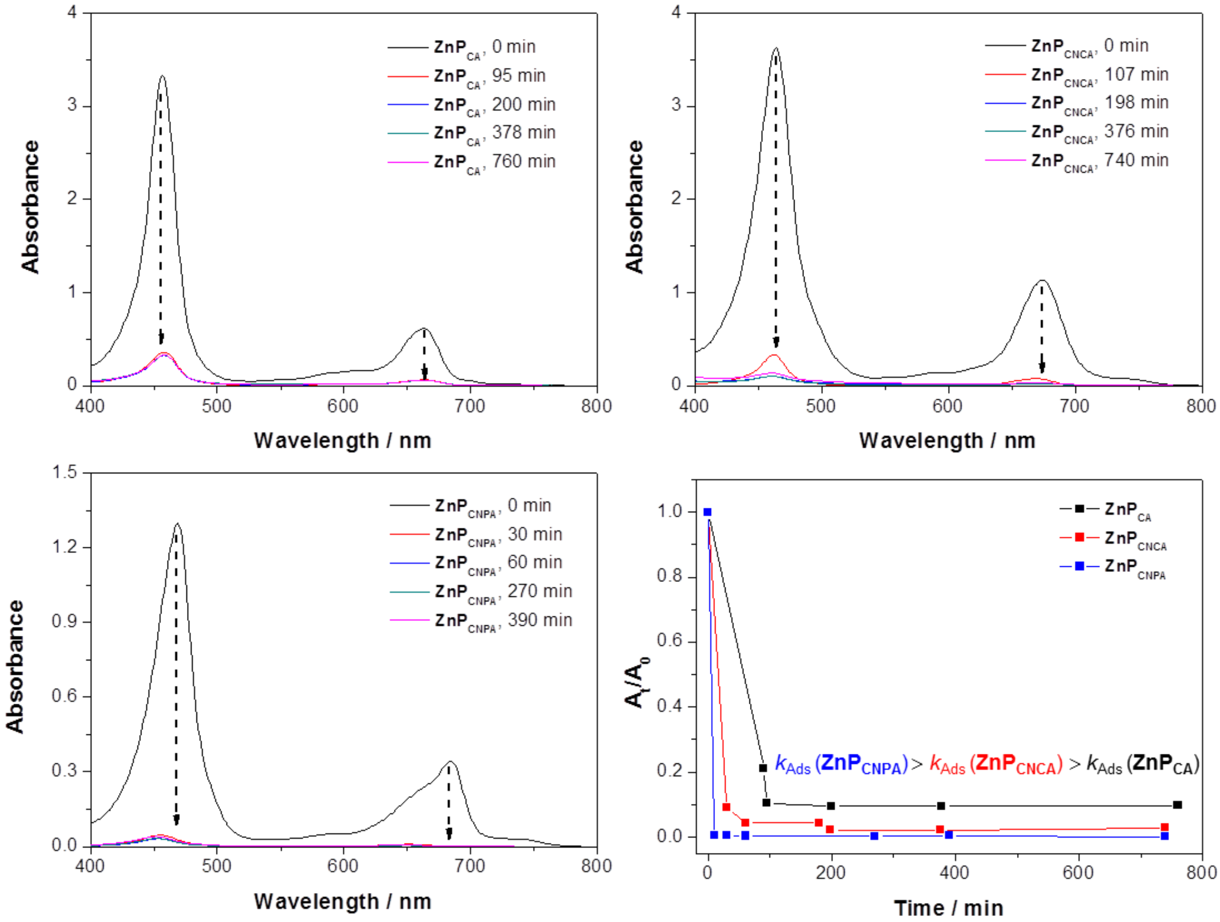

Figure S31. Absorption comparison of **ZnPs** solution (0.37 mM) before and after adsorption process with TiO_2 particles. Relative A_t/A_0 absorbance of **ZnPs** at 670 nm after soaking in DMF containing 10 mg TiO_2 particles.

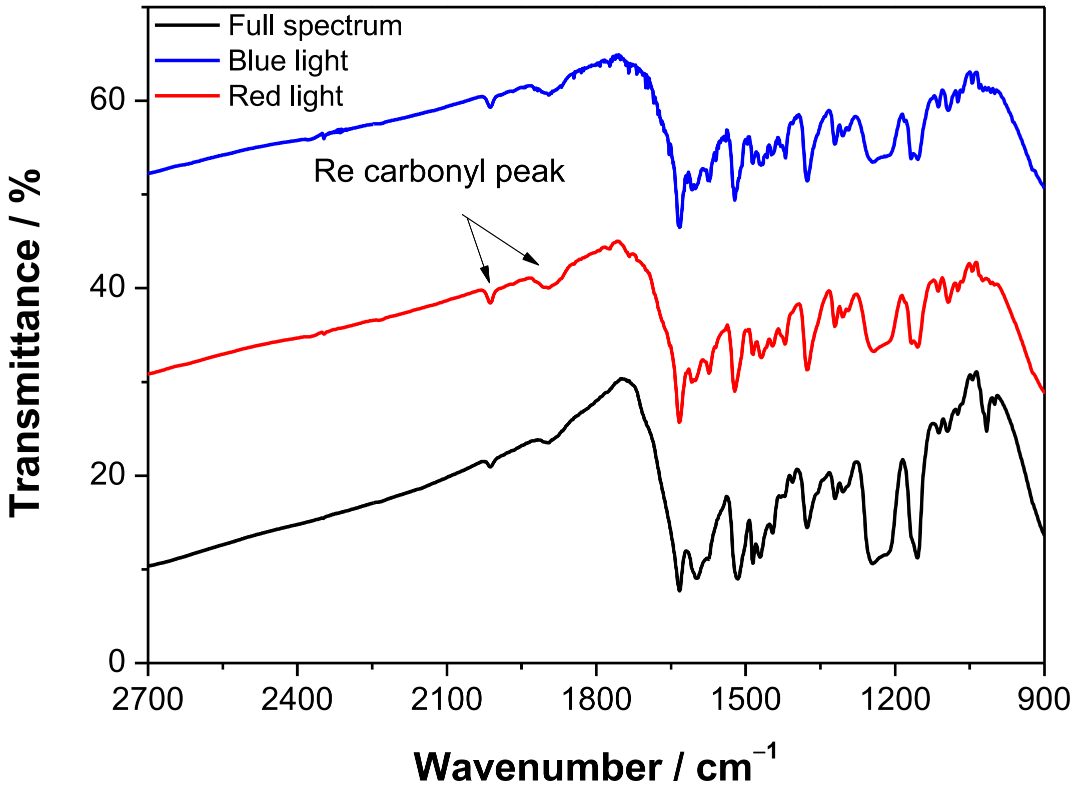

Figure S32. IR spectra comparison of **ZnP$_{\text{CNPA}}$-**|TiO_2|**-ReC** in KBr disks (sample:KBr ≈ 1:100) after 10 h photocatalysis with different wavelength irradiation.

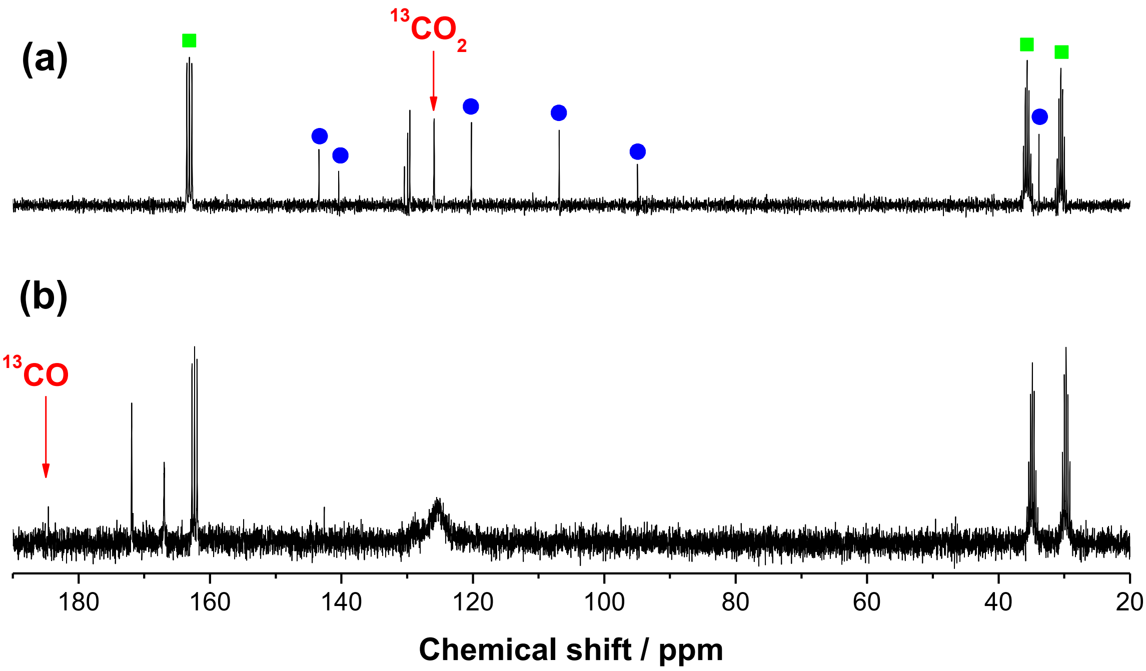

Figure S33. ^{13}C NMR spectra before (a) and after (b) 10 h irradiation in CO_2-saturated DMF-d_7 solvent containing 10 mg of **ZnP$_{CNCA}$**-|TiO_2|-**ReC** dispersion and 0.1 M BIH; irradiation at >400 nm. The symbols ■ and ● represent the peaks of DMF and BIH, respectively.

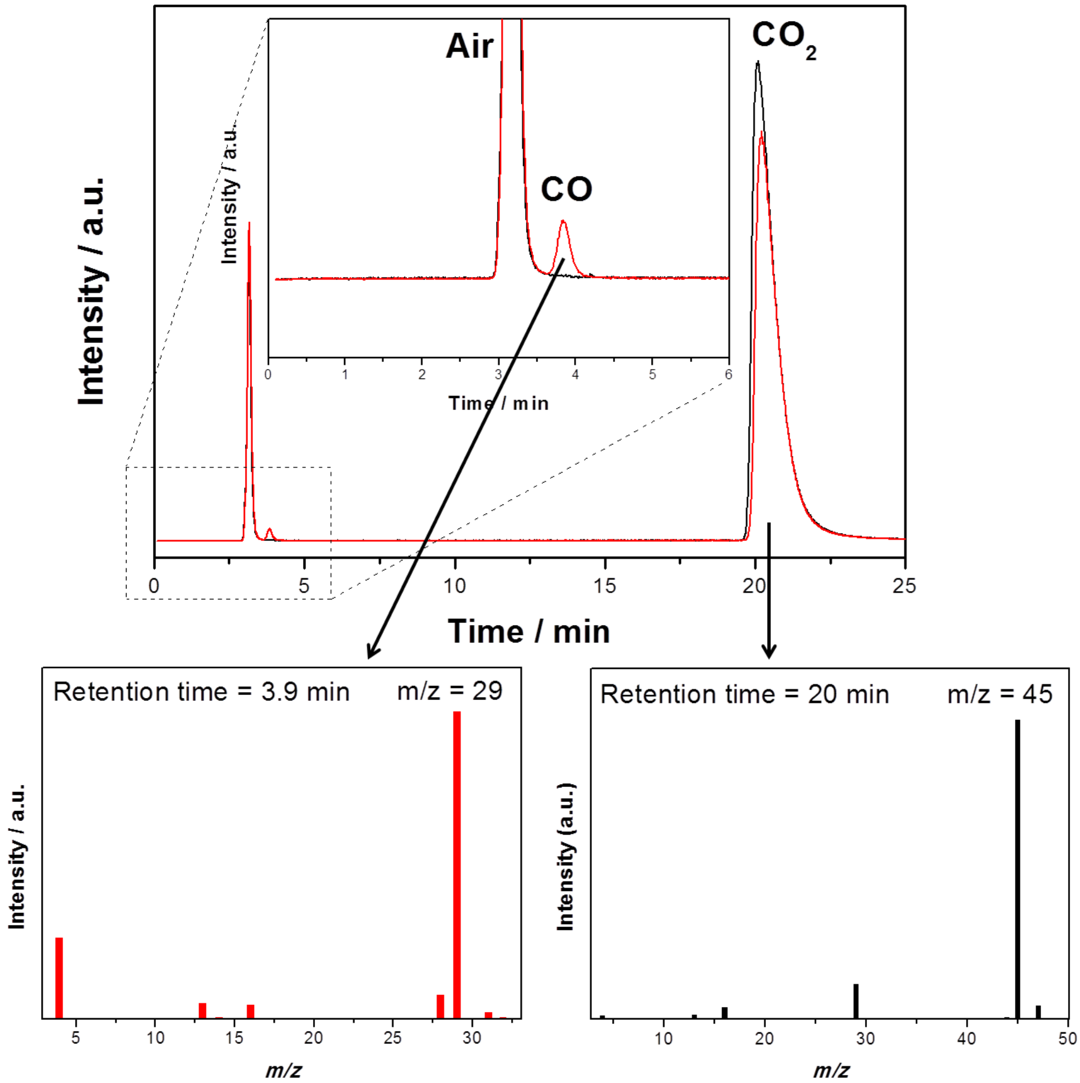

Figure S34. GC spectrum of gas in the reaction vessel before irradiation (black line), after irradiation (red line), and MS spectra of each retention times: GC-MS spectra was measured by Agilent Technologies 7890A GC equipped with 5975C inert MSD with Triple-Axis detector using a SUPELCO Carboxen™ 1010 PLOT Fused Silica Capillary column.

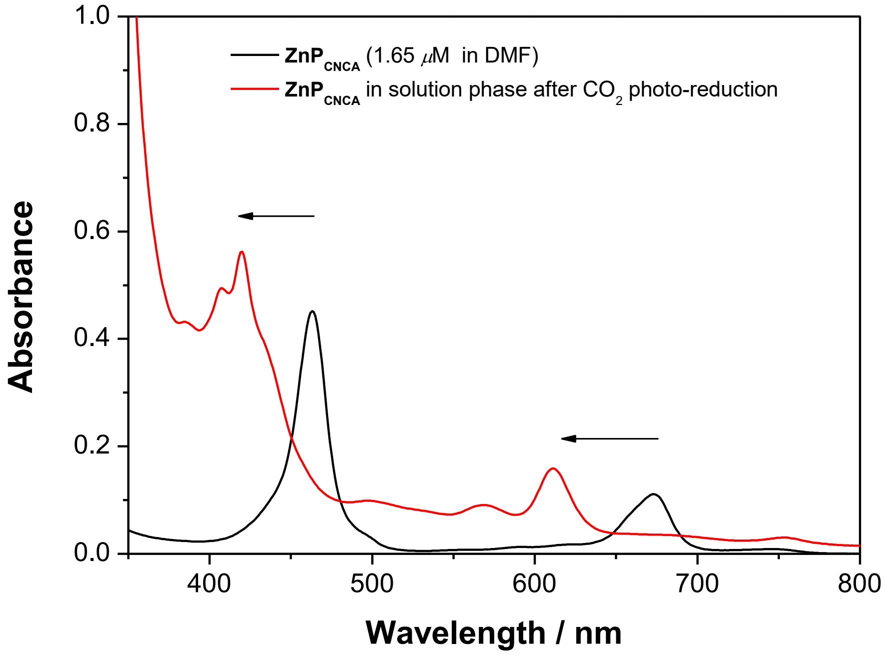

Figure S35. Absorption comparison of 1.65 μM **ZnP$_{CNCA}$** in DMF (black line) and supernatant liquid separated after photocatalysis (red line).

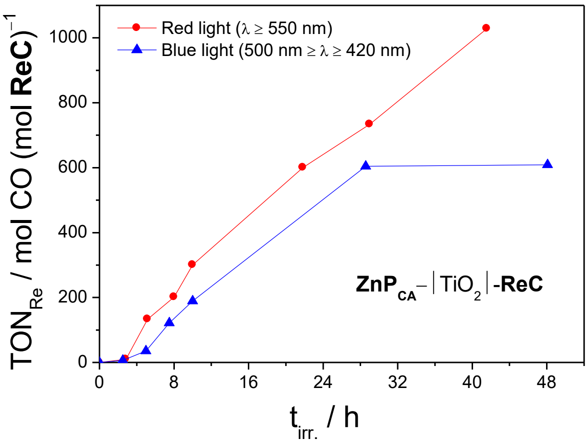

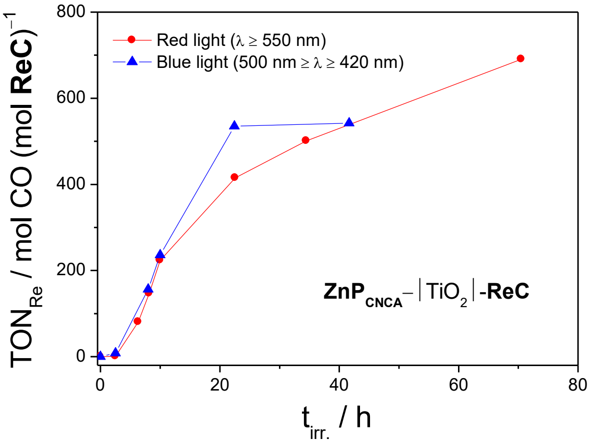

Figure S36. Time courses of CO formation for **ZnP$_{CA}$-**|TiO_2|**-ReC** hybrid (left) and **ZnP$_{CNCA}$-**|TiO_2|**-ReC** hybrid (right) in different wavelength range. All the light intensities are matched by 207 mW/cm^2 of irradiance.

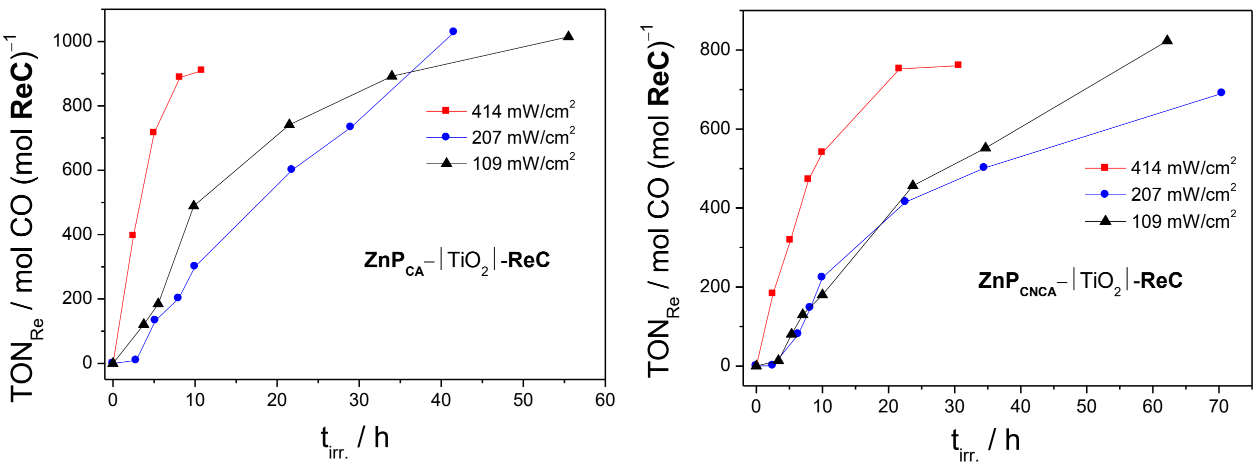

Figure S37. Time courses of CO formation for **ZnP$_{CA}$-**|TiO_2|**-ReC** (left) and **ZnP$_{CNCA}$-**|TiO_2|**-ReC** (right) hybrid by irradiation at >550 nm with variation of light intensity (109, 207, and 414 mW/cm^2).

Femtosecond Time-resolved Fluorescence Measurement: Light source was a home-made cavity dumped Kerr lens mode-locked Ti:sapphire oscillator operating at 1 MHz. The center wavelength and pulse duration were 830 nm and 25 fs, respectively. Femtosecond time-resolved fluorescence (TRF) was measured by the non-collinear fluorescence upconversion method. Pump pulses at 415 nm were generated by the SHG in a 200 μm thick lithium triborate crystal. The residual fundamental was used as a gate pulse. The fluorescence and the gate pulse were mixed in a 500 μm thick BBO crystal to generate the sum frequency radiation in a noncollinear phase-matching geometry with the external crossing angle set to 15°, where the effect of the group velocity mismatch and the phase front mismatch is minimized. Width of the cross-correlation between the pump and gate pulses was about 120 fs. Solution samples in DMF was prepared in a 200 μm path cuvette. Film sample, **ZnPs** adsorbed on TiO_2 nanoparticle, was prepared on an optical quality window and was mounted on a home-made shaking stage to minimize photodamage. All the experiments were carried out at ambient temperature.

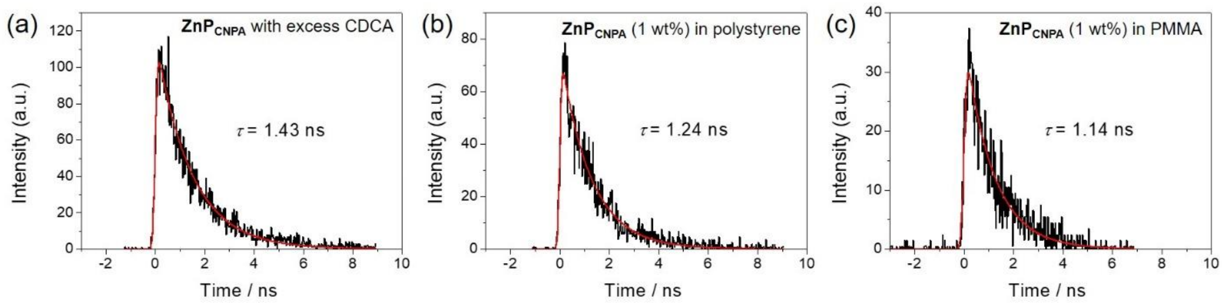

Figure S38. Time-resolved fluorescence signals of **ZnP$_{\mathbf{CNPA}}$** film with a large excess of CDCA (>1000 equiv) (a), **ZnP$_{\mathbf{CNPA}}$**-polystyrene (PS) film with 1 wt% **ZnP$_{\mathbf{CNPA}}$** (b), and **ZnP$_{\mathbf{CNPA}}$**-PMMA film with 1 wt% **ZnP$_{\mathbf{CNPA}}$** (c).

Table S1. Multiexponential nonlinear least square fit results for the time resolved fluorescence signals. Negative amplitude denotes rise component.

Sample	λ (nm)	A_1	τ_1 (fs)	A_1	τ_2 (ps)
ZnP$_{\mathbf{CNPA}}$ in DMF	490	100	143		
	650	–37	140	63	>1 ns
ZnP$_{\mathbf{CNPA}}$-|TiO_2	490	100	125		
	650	–29	140	71	1.1

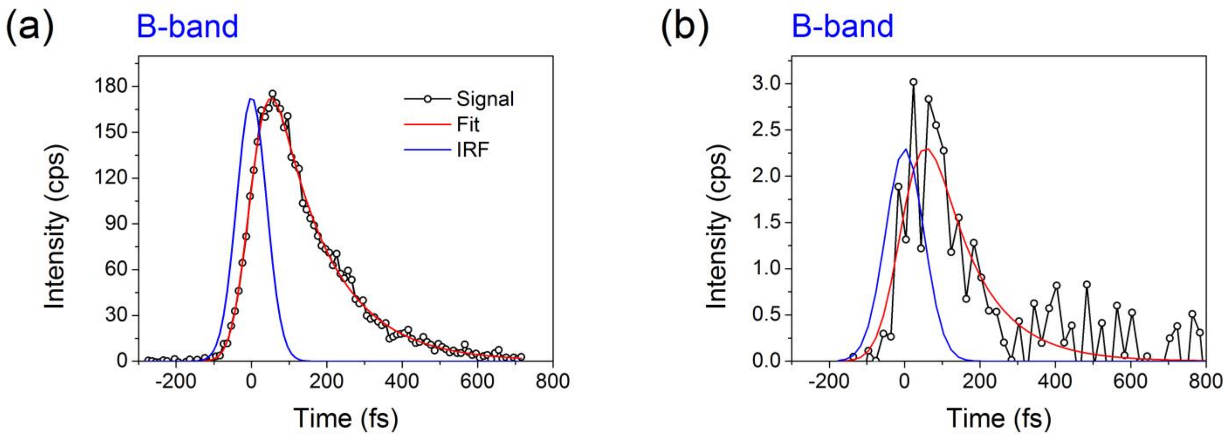

Figure S39. Time-resolved fluorescence signals of **ZnP$_{\mathbf{CNPA}}$** dissolved in DMF (a) and **ZnP$_{\mathbf{CNPA}}$-**|TiO_2 film (b). Note that the blue line displays the instrument response function (IRF) of the up-conversion set-up.